Molecular Therapy
Original Article

METTL5-mediated 18S rRNA m^{6}A modification promotes oncogenic mRNA translation and intrahepatic cholangiocarcinoma progression

Zihao Dai,[1,9] Wanjie Zhu,[2,9] Yingdong Hou,[3,9] Xinyue Zhang,[4,9] Xuxin Ren,[4] Kai Lei,[1] Junbin Liao,[1] Haining Liu,[1] Zhihang Chen,[1] Sui Peng,[3,5,6] Shaoqiang Li,[1] Shuibin Lin,[7] and Ming Kuang[1,5,8]

[1]Center of Hepato-Pancreato-Biliary Surgery, The First Affiliated Hospital, Sun Yat-Sen University, Guangzhou, Guangdong Province, China; [2]Department of Gastroenterology, The Eighth Affiliated Hospital, Sun Yat-Sen University, Shenzhen, Guangdong Province, China; [3]Department of Gastroenterology and Hepatology, The First Affiliated Hospital, Sun Yat-Sen University, Guangzhou, Guangdong Province, China; [4]Cancer Center, The First Affiliated Hospital, Sun Yat-Sen University, Guangzhou, Guangdong Province, China; [5]Institute of Precision Medicine, The First Affiliated Hospital, Sun Yat-Sen University, Guangzhou, Guangdong Province, China; [6]Clinical Trials Unit, The First Affiliated Hospital, Sun Yat-Sen University, Guangzhou, Guangdong Province, China; [7]Center for Translational Medicine, The First Affiliated Hospital, Sun Yat-Sen University, Guangzhou, Guangdong Province, China; [8]Zhongshan School of Medicine, Sun Yat-Sen University, Guangzhou, Guangdong Province, China

Intrahepatic cholangiocarcinoma (ICC) is a deadly cancer with rapid tumor progression. While hyperactive mRNA translation caused by mis-regulated mRNA or tRNA modifications promotes ICC development, the role of rRNA modifications remains elusive. Here, we found that 18S rRNA m^{6}A modification and its methyltransferase METTL5 were aberrantly upregulated in ICC and associated with poorer survival (log rank test, $p < 0.05$). We further revealed the critical role of METTL5-mediated 18S rRNA m^{6}A modification in regulation of ICC cell growth and metastasis using loss- and gain-of function assays *in vitro* and *in vivo*. The oncogenic function of METTL5 is corroborated using liver-specific knockout and overexpression ICC mouse models. Mechanistically, METTL5 depletion impairs 18S rRNA m^{6}A modification that hampers ribosome synthesis and inhibits translation of G-quadruplex-containing mRNAs that are enriched in the transforming growth factor (TGF)-β pathway. Our study uncovers the important role of METTL5-mediated 18S rRNA m^{6}A modification in ICC and unravels the mechanism of rRNA m^{6}A modification-mediated oncogenic mRNA translation control.

INTRODUCTION

Intrahepatic cholangiocarcinoma (ICC) accounts for 10%–20% of liver cancer, with increasing incidence in developed countries.[1,2] Most of ICC patients are diagnosed at advanced disease stage due to the rapid tumor progression. Advanced ICC is highly lethal even under aggressive chemotherapy, with overall survival less than 12 months. Up to now, there is only one targeted drug (FGF12 receptor inhibitor) selectively used in a small subset of ICC patients.[3] As such, understanding the mechanism governing the ICC progression is critical for promoting precise and effective targeted therapy for ICC.

Mis-regulated mRNA translation by abnormal RNA modifications has emerged as a new driving factor of cancer progression.[4,5] For example, m^{6}A modification in mRNA plays essential functions in promoting the stability and translation of oncogenic transcripts, resulting in tumor growth and recurrence.[6,7] In addition, accumulating studies have showed that modifications on tRNAs can drive tumor development in various cancers, including ICC.[8–10] Similar to mRNA and tRNA, ribosomal RNA (rRNA) also contains abundant modifications. Currently, more than 130 modifications have been identified in human rRNA at approximately 210 sites.[11] rRNA modifications in the ribosome translation machine are subjected to the functionally important regions and are linked to ribosome biogenesis and protein synthesis.[12] Some rRNA modifications, such as DKC1-mediated rRNA pseudouridylation, have been implicated in regulation of organ development and cancer biology.[13,14] In addition to controlling human physiology, rRNA methylation is also functionally crucial to plant growth.[15] For instance, chloroplast mraW-like (CMAL) methyltransferase-mediated N^4-methylcytidine methylation in 16S chloroplast rRNA is responsible for chloroplast biogenesis and photosynthesis. A mutant of CMAL reduced chloroplast biogenesis, altered photosynthetic activity, and stunted growth.[16] These studies indicate that rRNA modifications could have important functions in a wide range of physiological and

Received 19 May 2023; accepted 15 September 2023;
https://doi.org/10.1016/j.ymthe.2023.09.014.

[9]These author contributed equally

Correspondence: Shaoqiang Li, Center of Hepato-Pancreato-Biliary Surgery, The First Affiliated Hospital, Sun Yat-Sen University, Guangzhou, Guangdong Province, China.
E-mail: lishaoq@mail.sysu.edu.cn
Correspondence: Shuibin Lin, Center for Translational Medicine, The First Affiliated Hospital, Sun Yat-Sen University, Guangzhou, Guangdong Province, China.
E-mail: linshb6@mail.sysu.edu.cn
Correspondence: Ming Kuang, Center of Hepato-Pancreato-Biliary Surgery, The First Affiliated Hospital, Sun Yat-Sen University, Guangzhou, Guangdong Province, China.
E-mail: kuangm@mail.sysu.edu.cn

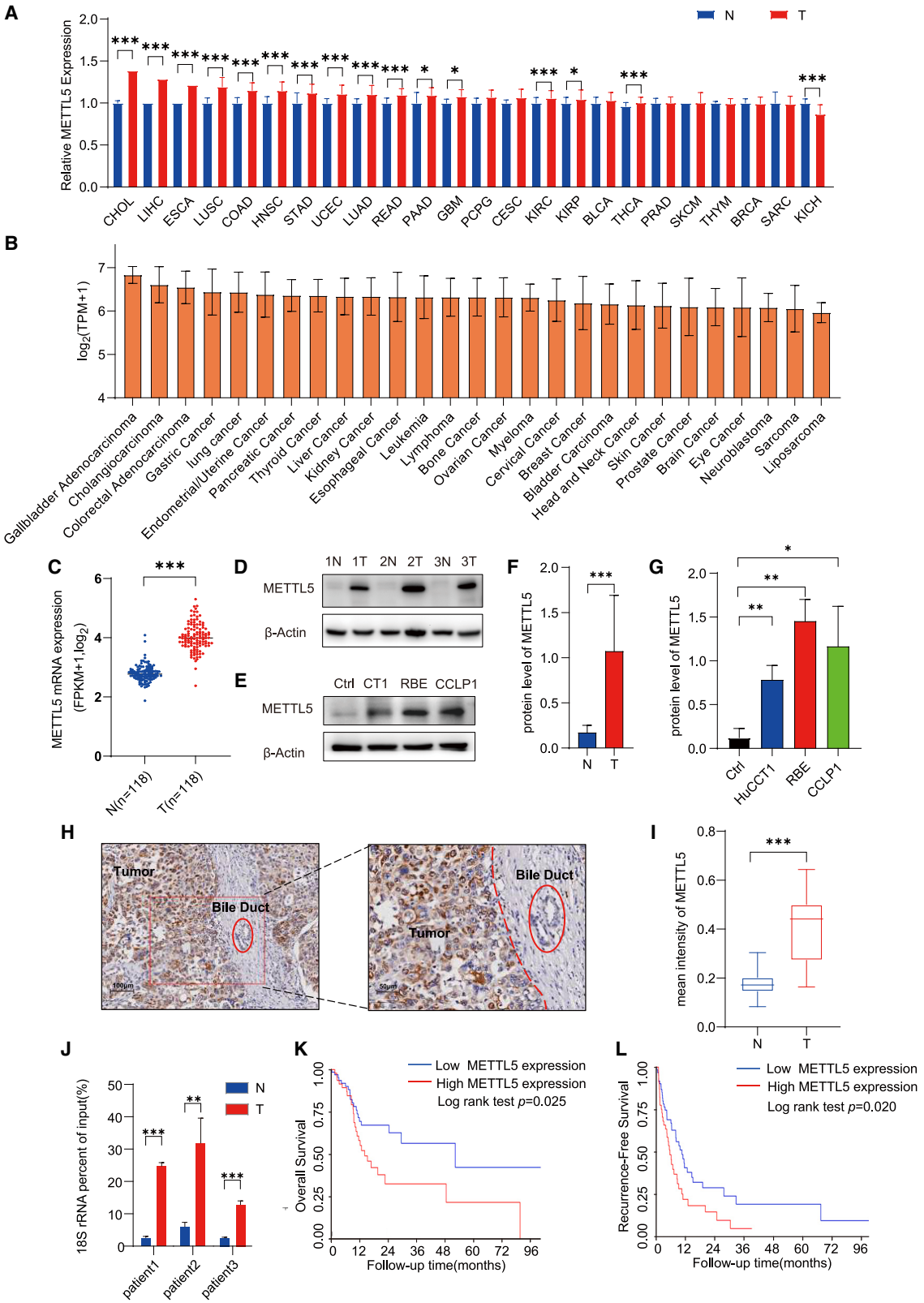

(legend on next page)

pathological processes in different species; however, our understanding of their roles still remains limited.

The m^{6}A is one of the most abundant rRNA modifications and is ubiquitously presented in human, worms, plants, etc.[17–19] Two rRNA m^{6}A modifications in humans so far have been identified: A4220 on 28S rRNA and A1832 on 18S rRNA.[20,21] Recent studies have revealed that rRNA m^{6}A modifications could promote mRNA translation and therefore are essential for fast-growing cells, including stem cells and cancer cells.[19,22–25] ICC is a highly lethal malignancy characterized by rapid tumor growth and metastasis. Previous studies have unraveled the importance of mRNA and tRNA modifications in regulation of ICC progression.[8,26,27] Nevertheless, the function of rRNA m^{6}A modification in ICC and the underlying mechanism remain largely unknown.

In the present study, we revealed that the 18S rRNA m^{6}A methyltransferase METTL5 is aberrantly overexpressed in ICC tumor and associated with poor survival. Impaired 18S m^{6}A modification significantly diminished the ICC growth and metastasis *in vitro* and *in vivo*. Mechanistically, loss of METTL5 preferentially affected the translation of those transcripts containing G-quadruplex (G4) motifs enriched in oncogenic signals such as transforming growth factor (TGF)-β pathways that significantly inhibited ICC progression. Our data uncover an important function of METTL5-mediated 18S rRNA m^{6}A modification in regulation of ICC progression and provide substantial evidence to support the novel link between rRNA modifications and cancer development.

RESULTS

The 18S rRNA m^{6}A methyltransferase METTL5 is upregulated in ICC and correlates with poor survival

To explore the potential role of METTL5 in cancer progression, we first examined the expression pattern of METTL5 across 24 solid cancer types using The Cancer Genome Atlas (TCGA) database. We found that METTL5 was overexpressed in 15 of 24 tumor types (62.5%) (Figure 1A). Notably, ICC (CHOL) was the top (ranked first) METTL5-upregulated tumor among all indicated tumor types in TCGA database (Figure 1A; CHOL samples: T = 34, N = 8). Besides, we found that METTL5 level was predominantly elevated among various m^{6}A methyltransferase in ICC (Figure S1). To corroborate the relation between METTL5 and cancers, we next determined the expression level of METTL5 in different cancer cells using the DepMap portal, a well-established database consisting of reliable data of nearly 3,000 cancer cell lines. Consistent with TCGA result, METTL5 was also highly upregulated in cholangiocarcinoma cells (ranked second) (Figure 1B). To further verify the functional link of METTL5 in ICC, we analyzed RNA sequencing (RNA-seq) data of tumors and paired non-tumor tissues from 118 ICC patients (Table S1). In accordance with the observation from the online database, the mRNA level of METTL5 was significantly elevated in ICC tumors compared to paired non-tumor tissues (Figure 1C, $p < 0.001$; Table S2). We also employed western blot assay and confirmed that the protein level of METTL5 in both ICC tumors and cell lines was aberrantly upregulated (Figures 1D–1G). In addition, TRMT112, the important component of 18S rRNA m^{6}A catalytic complex, is also upregulated in ICC tumors (Figure S2). Immunohistochemistry (IHC) staining further showed a substantially higher expression level of METTL5 in ICCs relative to adjacent normal bile ducts (Figures 1H and 1I; mean staining intensity: 0.41 ± 0.14 vs. 0.18 ± 0.06, $p < 0.001$). Consistently, the 18S rRNA m^{6}A modification level was profoundly elevated in ICC tumors (Figure 1J). Kaplan-Meier analysis revealed that the patients with higher METTL5 expression had shorter overall survival time and developed more frequent tumor recurrence (Figures 1K and 1L; log rank test, $p < 0.05$). Collectively, these results strongly support that METTL5-mediated 18S rRNA m^{6}A modification could play important functions in ICC progression.

Deletion of METTL5 perturbs ICC growth and metastasis

To study the functions of METTL5 in ICC, we employed two common ICC cell lines (RBE and HuCCT1), and knocked out METTL5 expression using CRISPR-Cas9 lentiviral vectors. The knockout of METTL5 was confirmed by western blot assays (Figures 2A and 2B). The levels of TRMT112 and 18S rRNA m^{6}A modification were remarkably reduced upon METTL5 depletion (Figures 2C and S3). In particular, METTL5 knockout significantly reduced 18S rRNA m^{6}A modification at site 1832 as examined by the single-base elongation-and ligation-based qPCR amplification (SELECT) method (Figure S4). Mass spectrometry assays were employed to further verify that METTL5 depletion impaired 18S rRNA m^{6}A modification but

Figure 1. Elevated expression of methyltransferase METTL5 and 18S rRNA m^{6}A modification in a human ICC specimen

(A) The relative expression levels of METTL5 in tumors (red box) and adjacent normal tissues (blue box) in 24 cancer types in TCGA database. The fragments per kilobase of exon per million mapped fragments (FPKM) expression values in tumors were normalized to those in corresponding normal tissues. (B) The relative expression levels of METTL5 in 27 types of cancer cell line in the DepMap portal database. (C) Comparison of METTL5 mRNA level between tumors and adjacent normal tissues from 118 ICC patients using RNA-seq data. (D) Comparison of METTL5 protein level between tumors and adjacent normal tissues from 12 ICC patients using freshly frozen specimens. (E) Comparison of METTL5 protein level between ICC cell lines and normal bile duct cells. (F and G) The quantitative analysis of METTL5 protein levels in human ICC specimen (F, related to D) and ICC cell lines (G, related to E). (H and I) Comparison of METTL5 expression level between tumors and adjacent normal tissues from 12 ICC patients using freshly frozen specimens. Representative images of high and low levels of METTL5 in human ICC specimens were determined by IHC (H). The corresponding quantitative result is presented in (I). Scale bar, 100 μm (H, left); scale bar, 50 μm (H, right). (J) Comparison of m^{6}A fractions of 18S rRNA between tumors and adjacent normal tissues from 12 ICC patients examined by the m^{6}A-IP-qPCR method. (K and L) Correlation between METTL5 expression level and overall survival (K) or recurrence-free survival (L) of ICC patients. Stratification was based on the expression level as indicated by RNA-seq data. Higher METTL5 expression: patients with METTL5 expression level higher than the average level calculated from all of patients in tumors. Overall survival (OS): the interval between the first resection to the date of death resulting from any cause or to the date of the last follow-up visit. Recurrence-free survival: the interval from achieving treatment to the first recurrent tumor found radiologically. The survival fraction was analyzed by the Kaplan-Meier method. Data presented as mean ± SD. *$p < 0.05$, **$p < 0.01$, ***$p < 0.001$. N, adjacent normal tissues; T, tumors; CHOL, ICC in TCGA.

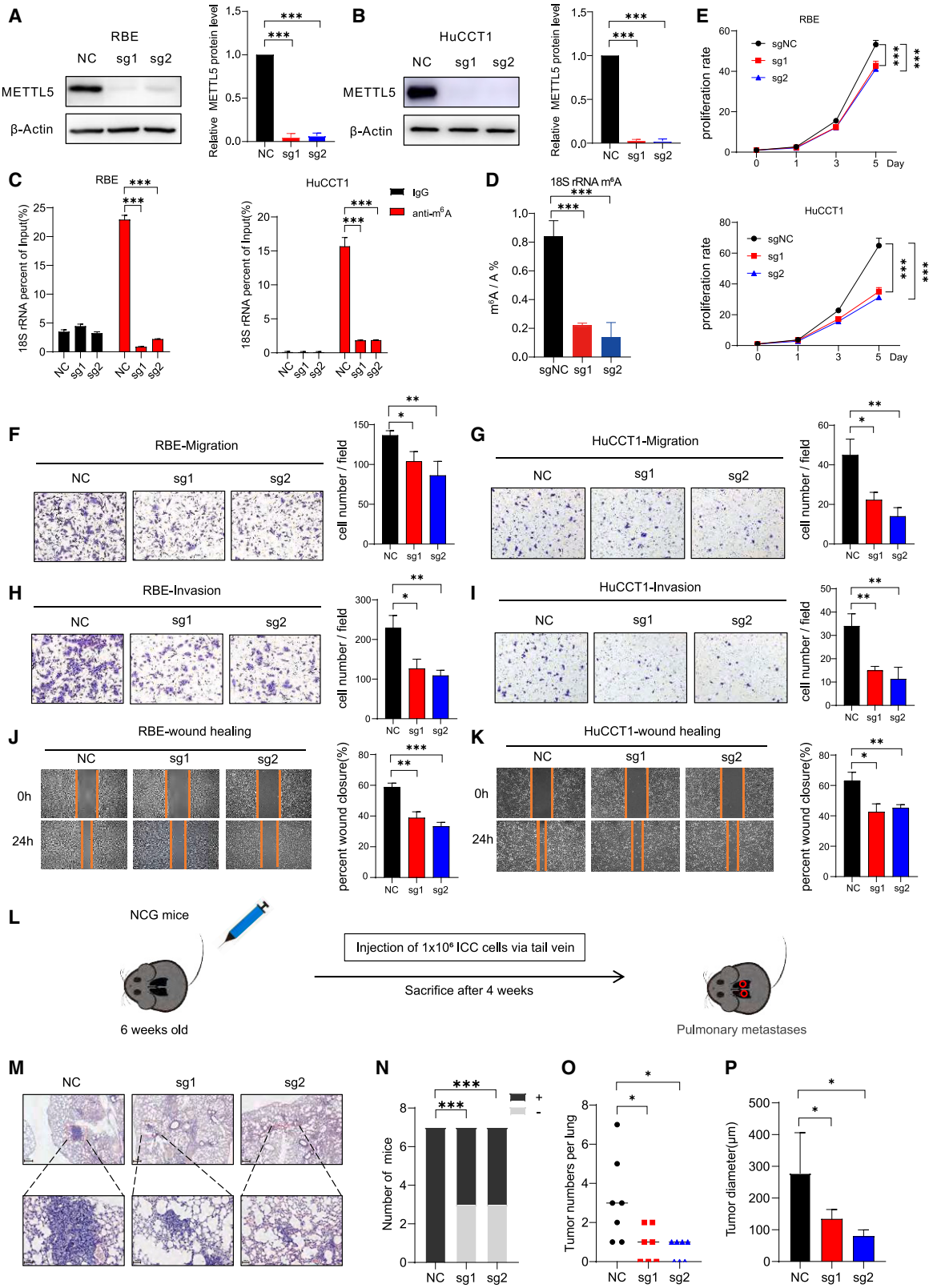

(legend on next page)

did not affect 28S rRNA m^6A modification and mRNA m^6A modification (Figures 2D and S5). Functionally, we found that loss of METTL5 significantly inhibited cell growth in both ICC cell lines (Figure 2E; $p < 0.001$). Moreover, knockout of METTL5 substantially suppressed the migratory (RBE, negative control [NC] vs. sg1 = 136.7 ± 5.8 vs. 104.0 ± 12.2, $p < 0.05$ and NC vs. sg2 = 136.7 ± 5.8 vs. 86.3 ± 17.6, $p < 0.01$; HuCCT1, NC vs. sg1 = 45.0 ± 8.0 vs. 22.3 ± 3.8, $p < 0.05$ and NC vs. sg2 = 45.0 ± 8.0 vs. 14.0 ± 4.4, $p < 0.01$) and invasive abilities (RBE, NC vs. sg1 = 229.5 ± 31.1 vs. 126.7 ± 23.6, $p < 0.05$ and NC vs. sg2 = 229.5 ± 31.1 vs. 109.2 ± 13.2, $p < 0.01$; HuCCT1, NC vs. sg1 = 34.0 ± 5.3 vs. 15.0 ± 5.7, $p < 0.01$ and NC vs. sg2 = 34.0 ± 5.3 vs. 11.3 ± 5.0, $p < 0.01$) of ICC cells (Figures 2F–2I). Wound-healing analysis further showed that METTL5 depletion profoundly attenuates the ICC cell migration (Figures 2J and 2K; wound closure, RBE, NC vs. sg1 = 58.8% ± 2.6% vs. 38.9% ± 3.9%, $p < 0.01$ and NC vs. sg2 = 58.8% ± 2.6% vs. 33.2% ± 2.6%, $p < 0.001$; HuCCT1, NC vs. sg1 = 63.1% ± 5.6% vs. 42.6% ± 5.3%, $p < 0.05$ and NC vs. sg2 = 63.1% ± 5.6% vs. 45.3% ± 2.1%, $p < 0.01$). Besides, similar functional inhibition could be also observed in both ICC cell lines upon METTL5 knockdown using short hairpin RNAs (shRNAs) (Figure S6), further solidifying the essential functions of METTL5 in ICC growth and metastasis.

We then sought to examine the *in vivo* oncogenic function of METTL5 using a lung metastasis mouse model. In this model, HuCCT1 cells with or without METTL5 depletion were separately injected into mouse bodies via tail vein injection, and the lung metastasis was analyzed in each group (Figure 2L). Compared with the controls, mice injected with METTL5-deleted HuCCT1 cells showed lower metastatic ratio (Figures 2M and 2N; NC vs. sg1 vs. sg2 = 100% vs. 57.1% vs. 57.1%, $p < 0.001$), developed fewer and smaller lung metastasis lesions (Figures 2O and 2P; tumor numbers, NC vs. sg1 vs. sg2 = 3.14 vs. 0.86 vs. 0.57, $p < 0.05$; tumor diameters, NC vs. sg1 vs. sg2 = 278.4 ± 127.9 μm vs. 134.3 ± 29.7 μm vs. 79.8 ± 20.1 μm, $p < 0.05$). Taken together, our *in vitro* and *in vivo* data disclose a critical role of METTL5 in regulation of ICC progression.

METTL5 regulates the translation of G4-containing mRNAs enriched in oncogenic TGF-β signal pathways

To interrogate how METTL5 regulated ICC progression, we first asked whether METTL5 depletion perturbs mRNA translation since 18S rRNA is an important component of ribosome 40S subunit and some other rRNA modifications have been implicated in regulation of ribosome maturation and gene expression.[19,28] We performed puromycin intake assays and found that METTL5 knockdown in RBE and HuCCT1 cells impairs the global mRNA translation (Figure 3A). We then examined the functional consequences of the METTL5-mediated m^6A modification on 18s rRNA. The RIP-qPCR data showed that loss of METTL5 did not diminish the 18S rRNA level (Figure S7) but reduced the binding between 18S rRNA and 40S subunit protein RPS29 (Figure 3B; $p < 0.001$), indicating an impediment of ribosome 40S subunit assembly. Consistently, the ribosome biosynthesis was also impaired, as shown by the reduced levels of ribosome proteins (Figures 3C and S8), which is in line with the observation of a previous report.[25]

We then performed ribosome nascent-chain complex-bound mRNA-seq (RNC-seq) to examine the alteration of mRNA translation upon METTL5 depletion in HuCCT1 cells. Analysis of RNC-seq data identified 3,964 transcripts with decreased translation ratio (TR) and 216 transcripts with increased TR (Figure 3D; Table S3). Due to the perturbations of 40S subunit and ribosome assembly upon METTL5 depletion, we proposed that mRNA G4 motifs could be a potential regulatory factor since the G4-containing mRNAs have been reported to be translationally inhibited by the stalled 40S ribosomal subunits.[29,30] Based on the identified G4 mRNA list from previous work (Table S4),[31] our RNC-seq data showed that 52.8% of the TR-down transcripts upon METTL5 depletion were G4 mRNAs, while only 3.2% of TR-up transcripts contained G4 structure (Figure 3E; chi-squared test, $p < 0.001$). In addition, we found that the TR of G4 mRNAs were lower upon METTL5 knockdown compared to the non-G4 mRNAs (Figure 3F; $p < 0.001$), further indicating the important role of G4 structure in regulation of METTL5-mediated mRNA translation control. Moreover, the length of 5′ UTR of TR-down transcripts tended to be shorter than the TR-up transcripts (Figure 3G; $p < 0.001$). Further analysis showed that shorter 5′ UTR length is linked to lower TR upon METTL5 depletion (Figure S9). This observation could possibly be explained by the established concept that the translation of mRNAs with shorter 5′ UTR is more susceptible to a reduction in ribosome levels. Collectively, these data demonstrate that METTL5-mediated 18S rRNA modification could regulate ribosome synthesis and translation of a subset of transcripts.

Figure 2. Loss of METTL5 hampers ICC progression *in vitro* and inhibits tumor metastasis *in vivo*

(A and B) Western blotting confirmation of METTL5 depletion using two independent lentiCRISPR-METTL5 plasmids in RBE (A) and HuCCT1 (B) cells. The bands are quantified in the right panels. (C) Comparison of the m^6A fraction levels of 18S rRNA between control and METTL5-depleted ICC cells using the m^6A-IP-qPCR method. (D) Validation of the alteration of the m^6A fraction levels of 18S rRNA between control and METTL5-depleted ICC cells using the liquid chromatograph-mass spectrometer spectrometry method. (E) MTX assay examining the growth in METTL5-depleted and control RBE (left) and HuCCT1 (right) cells. (F and G) Cell migration analysis between METTL5-depleted and control RBE (F) and HuCCT1 (G) cells. Left panels: representative images. Right panels: quantitative data. (H and I) Cell invasion analysis between METTL5-depleted and control RBE (H) and HuCCT1 (I) cells. Left panels: representative images. Right panels: quantitative data. (J and K) Wound-healing assays between METTL5-depleted and control RBE (J) and HuCCT1 (K) cells. Left panels: representative images. Right panels: quantitative data. (L) The diagram of experiment design of caudal vein injection mouse metastasis model. (M) Representative images of lung metastatic lesions in NCG mice injected with METTL5-depleted and control HuCCT1 cells from caudal vein using H&E staining. N = 7. Scale bar, 1 mm (L, top). Scale bar, 100 μm (L, bottom). (N) Comparison of the number of mice with or without lung metastasis between METTL5-depleted and control group. (O) Comparison of the number of average metastatic lesions per lung in each mouse between METTL5-depleted and control group. (P) Comparison of the tumor diameter in NCG mice between METTL5-depleted and control group. Data presented as mean ± SD. *$p < 0.05$, **$p < 0.01$, ***$p < 0.001$ (one-way ANOVA; chi-squared test). sg1, single guide RNA (sgRNA)-METTL5-1; sg2, sgRNA-METTL5-2; NC, negative control sgRNA.

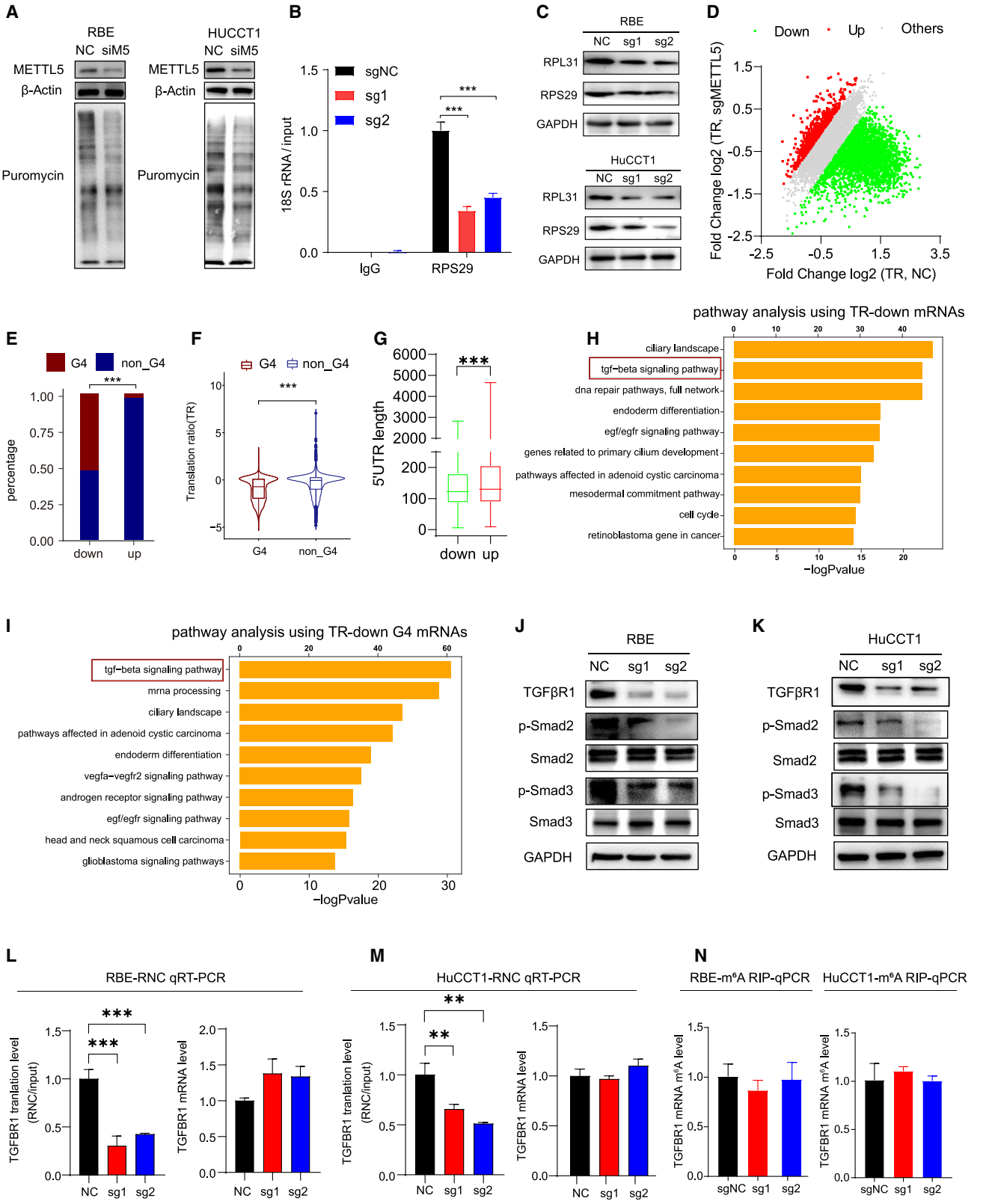

(legend on next page)

To further identify the key downstream targets of METTL5, Wikipathway cancer analysis was employed using the global mRNAs or G4 mRNAs with decreased TR in METTL5-depleted cells, respectively. Of note, TGF-β signal pathway is overlapped and significantly enriched in both datasets (Figures 3H and 3I). TGF-β pathway is a classic oncogenic signal for supporting cancer cell proliferation and metastasis. We found TGFBR1, a key regulator of TGF-β pathway,[32,33] was significantly downtranslated upon METTL5 knockdown (Table S3), while it is also a well-known G4-containing mRNA,[31] and we thus selected TGFBR1 as a representative target of METTL5-mediated 18S rRNA m^6A modification. The western blot assays showed that loss of METTL5 significantly diminishes TGFBR1 protein level. Consistently, the activation of corresponding downstream signals was also inhibited, as shown by the reduced phosphorylation of Smad2 and Smad3 (Figures 3J, 3K, and S8). We then further performed RNC-qPCR assays and found that METTL5 depletion had little effect on the TGFBR1 mRNA level but significantly decreased its TR (Figures 3L and 3M). Of note, loss of METTL5 did not affect TGFBR1 mRNA m^6A modification level (Figure 3N). Together, our data uncover the unappreciated role of METTL5-mediated 18S rRNA m^6A modification in regulation of oncogenic mRNA translation via G4s in ICC.

Phenotype defect upon METTL5 depletion is partially abrogated by TGFBR1 overexpression in ICC

To functionally validate the link between METTL5 and the translation-affected oncogenic mRNAs, we performed rescue assays by overexpressing TGFBR1 in METTL5-deleted RBE and HuCCT1 cells. The western blot data showed significant overexpression of TGFBR1 and knockdown of METTL5 in both cell lines (Figures 4A–4F). Notably, while knockdown of METTL5 remarkably suppressed ICC cell migration and invasion, ectopic expression of TGFBR1 could partially restore the ICC cell migratory (Figures 4G–4J; RBE, sgNC+oeNC vs. sgNC+oeR1 vs. sgM5+oeNC vs. sgM5+oeR1 = 155.3 ± 5.0 vs. 168.0 ± 2.0 vs. 33.3 ± 4.2 vs. 72.3 ± 2.5; HuCCT1, sgNC+oeNC vs. sgNC+oeR1 vs. sgM5+oeNC vs. sgM5+oeR1 = 170.3 ± 2.5 vs. 190.0 ± 10.0 vs. 28.0 ± 2.0 vs. 90.0 ± 10.1) and invasive abilities (Figures 4K–4N; RBE, sgNC+oeNC vs. sgNC+oeR1 vs. sgM5+oeNC vs. sgM5+oeR1 = 113.7 ± 3.2 vs. 121.3 ± 4.2 vs. 26.3 ± 1.5 vs. 54.0 ± 5.3; HuCCT1, sgNC+oeNC vs. sgNC+oeR1 vs. sgM5+oeNC vs. sgM5+oeR1 = 123.3 ± 6.1 vs. 145.3 ± 5.0 vs. 43.3 ± 6.1 vs. 87.7 ± 2.5), further corroborating the important target role of TGFBR1 upon METTL5 depletion. Altogether, these data further support that METTL5 deficiency disrupts the identified oncogenic mRNA expression that can regulate ICC progression.

Liver-specific knockout of Mettl5 inhibits ICC development *in vivo*

To further determine the oncogenic role of METTL5 in the regulation of ICC progression *in vivo*, we generated the *Alb-Cre*; $Mettl5^{fl/fl}$ (conditional knockout [cKO]) and $Mettl5^{fl/fl}$ (control [ctrl]) C57BL/6 mice. We then performed hydrodynamic transfection of AKT (myr-AKT) and Yap (YapS127A) plasmids to the abovementioned mice to established orthotopic ICC tumorigenesis models (Figure 5A).[8,34,35] Knockout of Mettl5 was validated by western blot (Figures 5B and 5C) and qRT-PCR assays (Figure 5D), respectively. By 6 weeks after transfection, the livers of control mice exhibited dramatic pathological enlargement, while no obvious volume alteration of livers was observed in Mettl5-cKO mice (Figures 5E and 5F). Consistently, the tumor burden, as indicated by the liver weight, was significantly decreased in Mettl5-cKO mice compared to that in control mice (Figures 5G and 5H; liver weight, ctrl vs. cKO = 5.33 ± 2.7 g vs. 1.32 ± 0.15 g, $p < 0.01$). Hematoxylin and eosin (H&E) staining revealed that the control mice developed a large number of tumor lesions; however, strikingly, no tumors but only weak steatosis-like changes were found in the livers of Mettl5-cKO mice (Figures 5I and 5J). Histological analysis further revealed that CK19, a classic biomarker of ICC, was highly expressed in these tumor lesions (Figure 5K, staining intensity, ctrl vs. cKO = 0.16 ± 0.03 vs. 0.10 ± 0.02, $p < 0.001$; Figure S10). Notably, the tumors in control mice showed a high proliferative activity, as indicated by the significantly increased number of Ki67-positive cells (Figure 5L, staining intensity, ctrl vs. cKO = 0.02 ± 0.005 vs. 0.007 ± 0.002, $p < 0.001$; Figure S10). Consistently, the protein levels of downstream target TGFBR1 and ribosomal proteins RPL31 and RPS29 were decreased in the Mettl5-cKO mice (Figures 5M and S11), while their mRNA levels remained unchanged (Figure 5N). Overall, these data provide *bona fide* evidence to further clarify the oncogenic function

Figure 3. METTL5 regulates oncogenic mRNAs translation via G4s

(A) Puromycin intake assays examining global mRNA translation of RBE (left) and HuCCT1 (right) cells with or without METTL5 depletion using the corresponding siRNA. Total protein samples were detected by western blot using anti-puromycin antibody. (B) Examination of the binding between 18S rRNA and ribosome 40S subunit protein RPS29 in control and METTL5-depleted HuCCT1 cell. (C) Western blot assays examining the ribosome protein levels of RBE (top) and HuCCT1 (bottom) cells with or without METTL5 depletion using the lentiCRISPR-sgRNA-METTL5 system. (D) Scatterplot of TR alteration in METTL5-depleted RBE cells compared to the control cells. TRs were calculated by dividing the ribosome binding transcripts signals to the input RNA-seq signals. Down: transcripts with decreased TR upon METTL5 depletion. Up: transcripts with upregulated TR upon METTL5 depletion. Others: transcripts with stable TR upon METTL5 depletion. (E) The quantitative comparison of ratios of G4-containing mRNAs between the TR-down and TR-up transcripts upon METTL5 depletion. The list of G4-containing mRNAs originated from the previous study. (F) Violin plot of TR alteration of mRNAs with or without G4s upon METTL5 depletion. (G) The quantitative comparison of 5′-UTR length of mRNAs between the TR-down and TR-up transcripts upon METTL5 depletion. (H) Wikipathway analysis of the TR-down mRNAs upon METTL5 depletion. (I) Wikipathway analysis of the GG4-containing TR-down mRNAs upon METTL5 depletion. (J and K) Validation of the expression or activation of candidate downstream signals by western blot assays in RBE (J) and HuCCT1 (K) cells upon METTL5 depletion. (L and M) qRT-PCR analysis of representative genes of RNC and input samples in HuCCT1 and RBE cells. Left: TR of indicated transcripts. Right: mRNA levels of indicated transcripts. (N) Examination of the m^6A modification levels of TGFBR1 mRNA between the control and METTL5-depleted ICC cells using the m^6A RIP-qPCR method. Data presented as mean ± SD. $^{**}p < 0.01$, $^{***}p < 0.001$ (chi-squared test; Wilcoxon rank-sum test; one-way ANOVA). NC, negative control; siM5, siMETTL5; sg1, sgRNA-METTL5-1; sg2, sgRNA-METTL5-2.

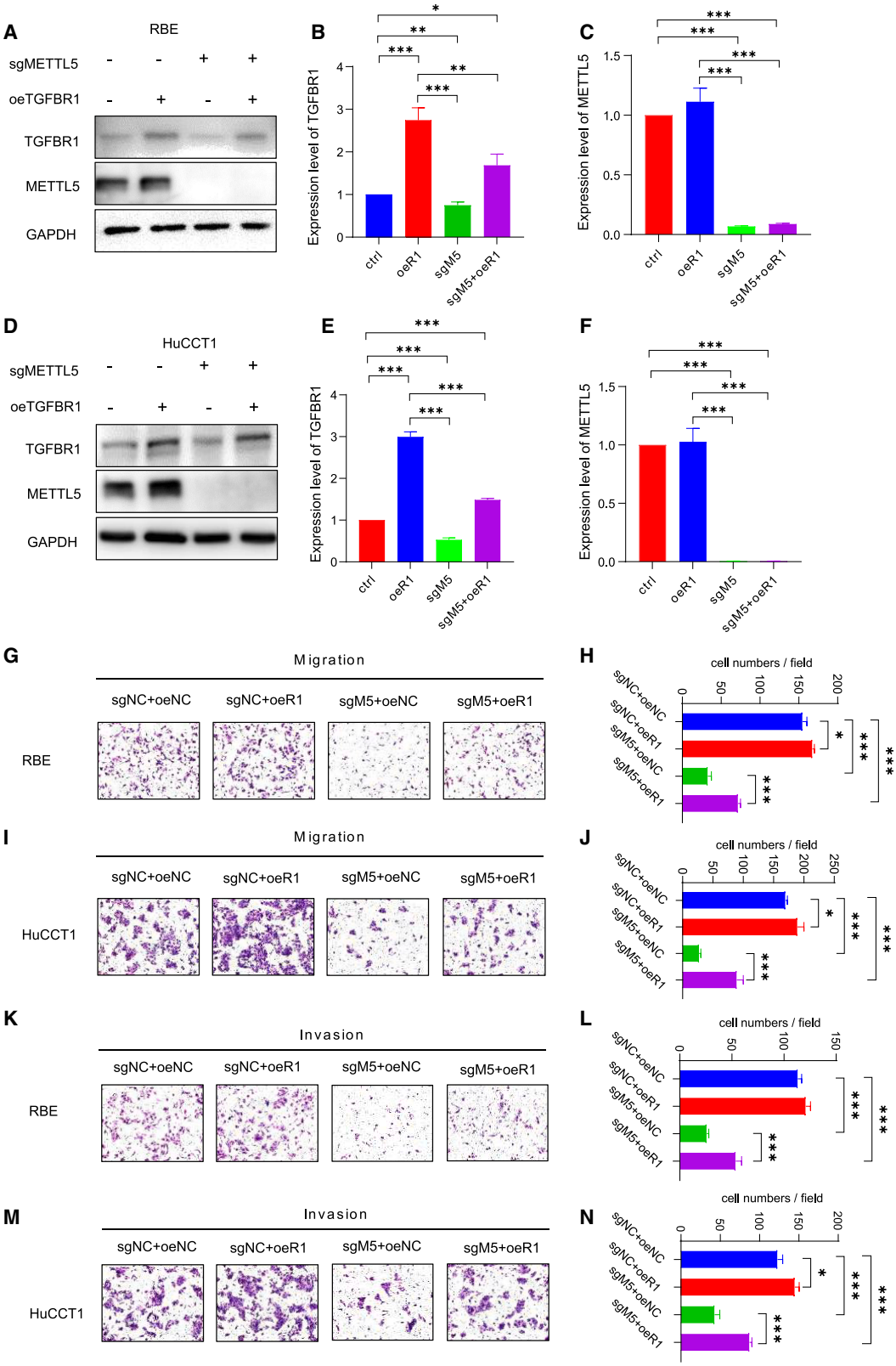

(legend on next page)

of Mettl5-mediated 18S rRNA m^6A modification in fueling ICC development *in vivo*.

Overexpression of wild-type METTL5, but not its methyltransferase inactive mutant, promotes ICC progression

Next, we performed gain-of-function studies to investigate the regulatory effect of METTL5-mediated 18S rRNA m^6A modification in ICC. Of note, ectopic expression of wild-type (WT) METTL5 but not the catalytic-site-mutated METTL5 increased the expression levels of TGFBR1, RPL31, RPS29, and TRMT112 (Figures 6A, S12, and S13). Correspondingly, the level of 18S rRNA m^6A modification was significantly elevated upon WT METTL5 overexpression, whereas catalytically inactive METTL5 had little effect on the m^6A modification level (Figure 6B; $p < 0.001$). Functionally, overexpression of WT METTL5 significantly enhanced the ICC cell migration (Figures 6C and 6D; RBE, NC vs. WT = 94.3 ± 53.6 vs. 256.0 ± 34.9, $p < 0.05$ and WT vs. M5-mut = 256.0 ± 34.9 vs. 121.0 ± 39.1, $p < 0.05$; HuCCT1, NC vs. WT = 78.0 ± 12.0 vs. 198.7 ± 8.1, $p < 0.001$ and WT vs. M5-mut = 198.7 ± 8.1 vs. 139.0 ± 15.7, $p < 0.01$), invasion (Figures 6E and 6F; RBE, NC vs. WT = 26.5 ± 5.3 vs. 66.8 ± 9.1, $p < 0.001$ and WT vs. M5-mut = 66.8 ± 9.1 vs. 40.3 ± 2.5, $p < 0.01$; HuCCT1, NC vs. WT = 173.3 ± 19.4 vs. 281.0 ± 35.7, $p < 0.05$ and WT vs. M5-mut = 281.0 ± 35.7 vs. 177.3 ± 20.5, $p < 0.05$) and wound-healing ability (Figures 6G and 6H; wound closure, RBE, NC vs. WT = 33.8 ± 3.1 vs. 57.9 ± 1.2, $p < 0.001$ and WT vs. M5-mut = 57.9 ± 1.2 vs. 38.5 ± 1.1, $p < 0.001$; HuCCT1, NC vs. WT = 38.7 ± 2.0 vs. 59.9 ± 1.3, $p < 0.001$ and WT vs. M5-mut = 59.9 ± 1.3 vs. 33.8 ± 3.6, $p < 0.001$). Nevertheless, methyltransferase-inactive mutant METTL5 did not promote ICC progression. Collectively, these results demonstrate that the 18S rRNA m^6A methyltransferase activity is critical for METTL5's function in ICC progression.

Liver-specific overexpression of Mettl5 promotes *in vivo* ICC progression

To further verify the cancer-promoting functions of METTL5-mediated 18S rRNA m^6A modification in ICC, Mettl5 overexpression plasmids were co-injected with AKT/YapS127A plasmids to determine whether Mettl5 overexpression promotes ICC progression *in vivo* (Figure 7A). Overexpression of Mettl5 in mouse liver was validated after transfection (Figures 7B and S14). The protein level of Mettl5 was also elevated, accompanied with the upregulated expression of TGFBR1 and ribosomal proteins (Figures 7C and S14), indicating the reliability of this model. Notably, while AKT/YapS127A/Mettl5 (OEMettl5) mice developed heavy tumor burdens by 4 weeks after plasmid injection, only a few small tumors presented in the liver of AKT/YapS127A/empty vector (ctrl) mice (Figures 7D and 7E). Also, the liver weight of OEMettl5 mice was much higher than that of control mice (Figures 7F and 7G; liver weight, ctrl vs. OEMettl5 = 2.0 ± 0.69 g vs. 4.9 ± 2.0 g, $p < 0.05$). Pathological examination by H&E staining illustrated that OEMettl5 mice had a significantly increased number of tumor lesions compared to control mice (Figures 7H and 7I; tumor number, ctrl vs. OEMettl5 = 4.1 ± 2.3 vs. 15.0 ± 3.2, $p < 0.001$). In addition, IHC assay showed that tumor lesions in both OEMettl5 and control mice exhibited positive CK19 staining, demonstrating the tumorigenesis of ICC (Figures 7J and S15). Of note, the liver Mettl5-overexpressing mice showed a higher percentage of Ki67-positive cells than the control mice (Figure 7K, staining intensity, ctrl vs. OEMettl5 = 0.09 ± 0.02 vs. 0.15 ± 0.03, $p < 0.01$; Figure S15). Consistently, the ICC tumors in OEMettl5 mice conferred higher global mRNA translation level relative to the controls (Figure 7L), while the mRNA levels of TGFBR1 and ribosomal proteins remained unchanged (Figure 7M). Taken together, these results substantiate the crucial function of Mettl5 in promoting ICC progression *in vivo*.

DISCUSSION

Translational dysfunction caused by aberrant RNA modifications is a hallmark of cancers and emerges as a new regulatory layer of driving tumorigenesis. While mRNA and tRNA modifications have been extensively studied in cancers, little cancer-related function is known about the rRNA modifications. In fact, it has been reported that the rRNA modification is crucial for the stress resistance and lifespan in yeast and worms,[25,36] indicating an important role of rRNA modification in modulating biological activity. Recently, the 18S rRNA m^6A modification and its newly identified methyltransferase METTL5 have been connected to various developmental diseases; for example, mutation of METTL5 could led to autosomal-recessive intellectual disability and microcephaly.[37–39] In line with these observations, several studies have disclosed that METTL5-mediated 18S rRNA m^6A modification is essential for stem cell differentiation.[22,23,40] However, the role of METTL5-mediated 18S rRNA m^6A modification in cancers remains poorly understood. In the present study, we found that METTL5 is highly upregulated in multiple cancers, especially in ICC, and showed a close link to poor survival of ICC patients (log rank test, $p < 0.05$). These results are in accordance with the observation that METTL5 associates with the prognosis or drug resistance in cancers.[41–45] More importantly, we further provided substantial *in vitro* and *in vivo* data to reveal the critical role of METTL5-mediated 18S rRNA m^6A modification in promoting ICC cell growth and metastasis. The dramatic prevention of ICC tumorigenesis in *Mettl5* knockout mice and the rapid progression of ICC development in *Mettl5* overexpression mice strongly

Figure 4. Overexpression of downstream target TGFBR1 rescues the METTL5 depletion-induced ICC phenotype impairment

(A) Validation of theTGFBR1 overexpression in RBE cells with or without METTL5 depletion using western blot assays. (B and C) The quantitative data of TGFBR1 and METTL5 expression levels related to (A). (D) Validation of theTGFBR1 overexpression in HuCCT1 cells with or without METTL5 depletion using western blot assays. (E and F) The quantitative data of TGFBR1 and METTL5 expression levels related to (D). (G–J) Overexpression rescued the migration capacity of METTL5-depleted RBE (G and H) and HuCCT1 (I and J) cells. (G and I) The representative images. (H and J) The quantitative data. (K–N) Overexpression rescued the invasion capacity of METTL5-depleted RBE (K and L) and HuCCT1 (M and N) cells. (K and M) The representative images. (L and N) The quantitative data. Data presented as mean ± SD. *$p < 0.05$, **$p < 0.01$, ***$p < 0.001$ (one-way ANOVA). sgM5, sgRNA-METTL5-1; oeR1, overexpression of TGFBR1. Scale bar, 200 μm. All the assays were biologically repeated three times.

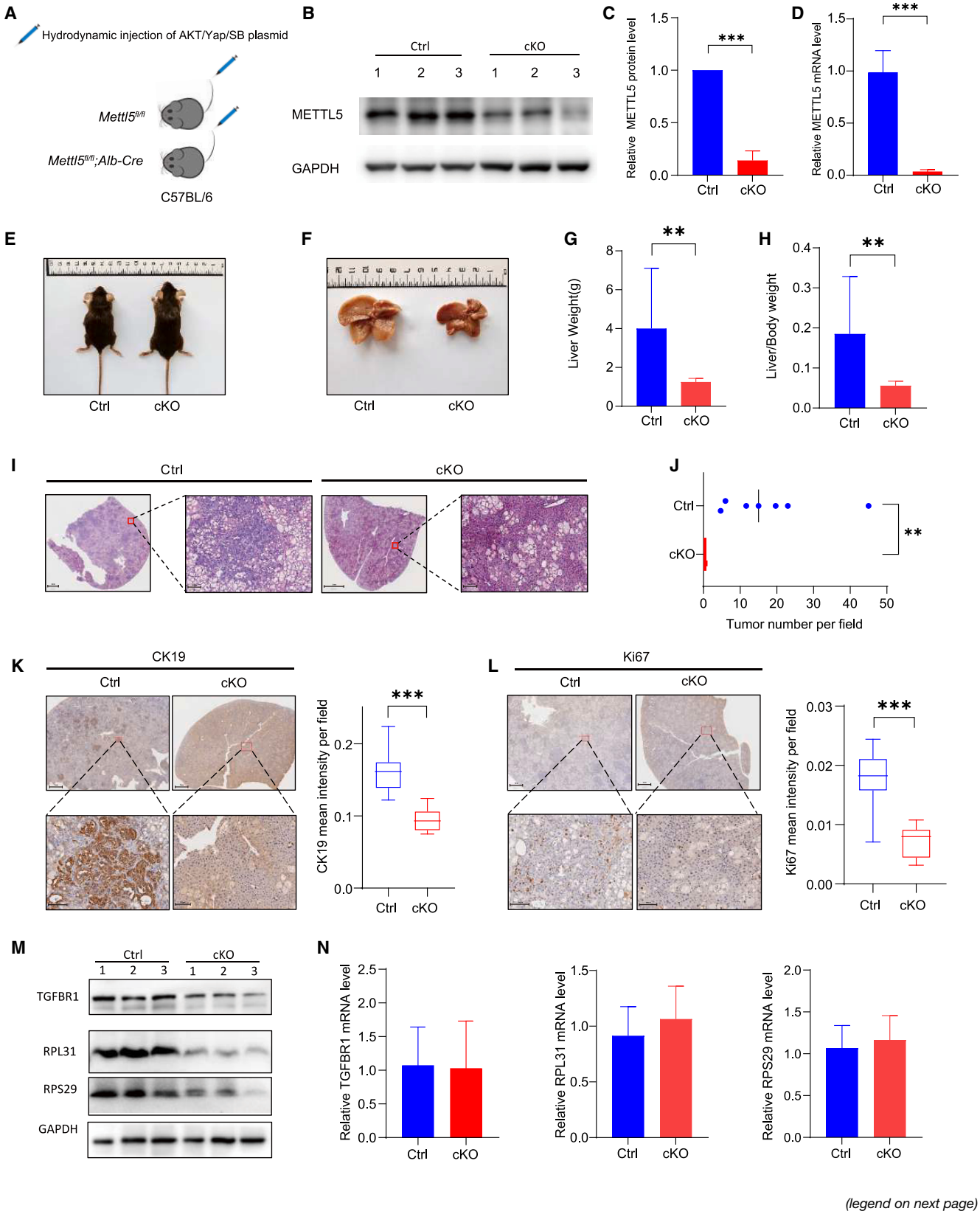

(legend on next page)

demonstrated the oncogenic function of METTL5-mediated 18S rRNA m^6A modification. Since the functional study of rRNA modifications in cancers is at the initial stage, our data support the importance of translation control in regulation of tumor progression modulated by rRNA modification level.

Despite the vital effect of METTL5-mediated 18S rRNA m^6A modification in cancers, the underlying mechanism remains poorly understood. In this study, we found that depletion of METTL5 significantly inhibits the global mRNA translation. This phenomenon is also supported by recent studies.[24,25] Accumulating studies have revealed that rRNA modifications are preferentially located in conserved functional sites, indicating that rRNA modifications play important roles in ribosome maturation, thus regulating the mRNA translation.[12,46] We found that loss of METTL5 decreases the 18S rRNA m^6A modification level and perturbs the ribosome synthesis. The alteration of ribosome level could affect mRNA translation. Previous studies have demonstrated that rRNA modifications could regulate a subset of transcripts by altering the affinity of ribosomes.[47–50] More recently, several studies have also revealed the internal ribosome entry sites (IRESs) or 5′-terminal oligopyrimidine (5′- TOP) motif-dependent mechanism in METTL5-mediated abnormal mRNA translation,[24,25] here, interestingly, we disclosed that part of the translation-affected mRNAs upon METTL5 knockdown share the G4 motif. These affected mRNAs and G4 mRNAs are both enriched in oncogenic TGF-β signals that are verified to be able to reverse the METTL5-mediated ICC phenotype change, raising an additional molecular mechanism regulated by METTL5. G4s are non-canonical structures organized in stacks of tetrads formed by G-rich RNA sequences in which four guanines are assembled in a planar arrangement.[51] It has been reported that G4s are associated with stalled 40S ribosomal subunits and reduced ribosome progression.[30] Indeed, 18S rRNA is the essential component of 40S subunit, and our data indicated that impaired METTL5-mediated 18S rRNA modification diminishes 40S subunit and ribosome synthesis. Therefore, the bias of G4-containing mRNA translation could be an explainable and understandable mechanism for METTL5-mediated ICC progression, which would help expand our understanding of the complex biology regulation of rRNA modifications and provide a more comprehensive framework for dissecting the abnormal mRNA translation in tumors.

ICC is a highly aggressive and fatal disease with active mis-regulated translation.[8,52] Several new drugs targeting mutation, e.g., IDH1 inhibitor, showed mild therapeutic efficacy and was restricted to a minor subset of patients.[53,54] Our previous study has indicated that targeting abnormal translation in ICC might be a promising strategy.[8] However, some attempts, such as mammalian target of rapamycin (mTOR) inhibitor, targeting translation machines are frequently associated with organ toxicity. Interestingly, knockout of METTL5 in certain human cells, including cancer cells, did not result in growth inhibition.[25,37] In our study, complete loss of METTL5 significantly suppresses ICC cell malignant phenotypes. These data implicate that METTL5-mediated functional alteration is complex and depends on different stress conditions. In this context, METTL5 might be an appealing target for translation inhibition in ICC that helps create safe therapeutic windows for ICC treatment.

In conclusion, we reveal the important oncogenic functions of METTL5-mediated 18S rRNA m^6A modification in ICC development and provide novel insight into the mechanism underlying the rRNA modification-G4-mediated oncogenic mRNA translation control. These findings could be of benefit for developing new strategies targeting abnormal translation for effective ICC treatment from the rRNA modification layer.

MATERIALS AND METHODS

Patient samples

Fresh ICC tumors and paired adjacent normal tissues were collected and were then frozen in liquid nitrogen from 12 ICC patients who had undergone surgical treatment in the First Affiliated Hospital of Sun Yat-Sen University. These specimens were used for examining the expression levels of METTL5 and 18S rRNA m^6A modification. In addition, total RNA samples of tumors and adjacent normal tissues from 118 ICC patients were available for high-throughput RNA-seq. Written informed consent had been obtained from each patient and ethical approval was obtained by the Institutional Review Board of the First Affiliated Hospital of Sun Yat-Sen University.

Cell lines and cell culture

The human ICC HuCCT1 cell line was obtained from Japan Health Sciences Foundation Resources Bank (Osaka, Japan). The human ICC RBE cell line and HEK293T cell line were purchased from Chinese Type Culture Collection (Shanghai, China). HuCCT1 and RBE cell lines were cultured in RPMI 1640 medium (GIBCO). The HEK293T cell line was cultured in DMEM medium (GIBCO). All culture media were supplemented with 10% fetal bovine serum (GIBCO, USA) and 1% penicillin and streptomycin (GIBCO, USA). All cell

Figure 5. Liver-specific knockout of Mettl5 suppresses ICC tumorigenesis

(A) The diagram of experiment design. (B and C) Protein level validation of conditional Mettl5 knockout (cKO) in mouse livers using western blot assays. A representative image is shown in (B). The quantitative data are present in (C). (D) mRNA level validation of Mettl5 knockout in mouse livers using qRT-PCR assays. (E) Comparison of tumor burden in control and cKO mice at 6 weeks after plasmids transfection. (F) Representative gross images of control and cKO mouse livers. (G and H) Comparison of tumor burden indicated by the liver weight (G) and the ratio of liver weight to body weight (H) between control and cKO mice. (I and J) Representative images of H&E staining of control and cKO mouse livers (I). The numbers of tumor lesions in control and cKO mouse livers were evaluated and compared (J). Scale bar, 2 mm (I, left); scale bar, 100 μm (I, right). (K and L) IHC staining of CK19 (K) and Ki67 (L) in control and cKO mouse livers (left). The corresponding statistical data are shown (right). Scale bar, 1 mm (K and L, top); scale bar, 100 μm (K and L, bottom). (M) The protein levels of TGFBR1 and ribosome proteins in control and cKO mouse livers. (N) The mRNA levels of TGFBR1 and ribosome proteins in control and cKO mouse livers. Data are presented as mean ± SD. $^{**}p < 0.01$, $^{***}p < 0.001$ (Student's t test). Ctrl, control; cKO, cKO of Mettl5.

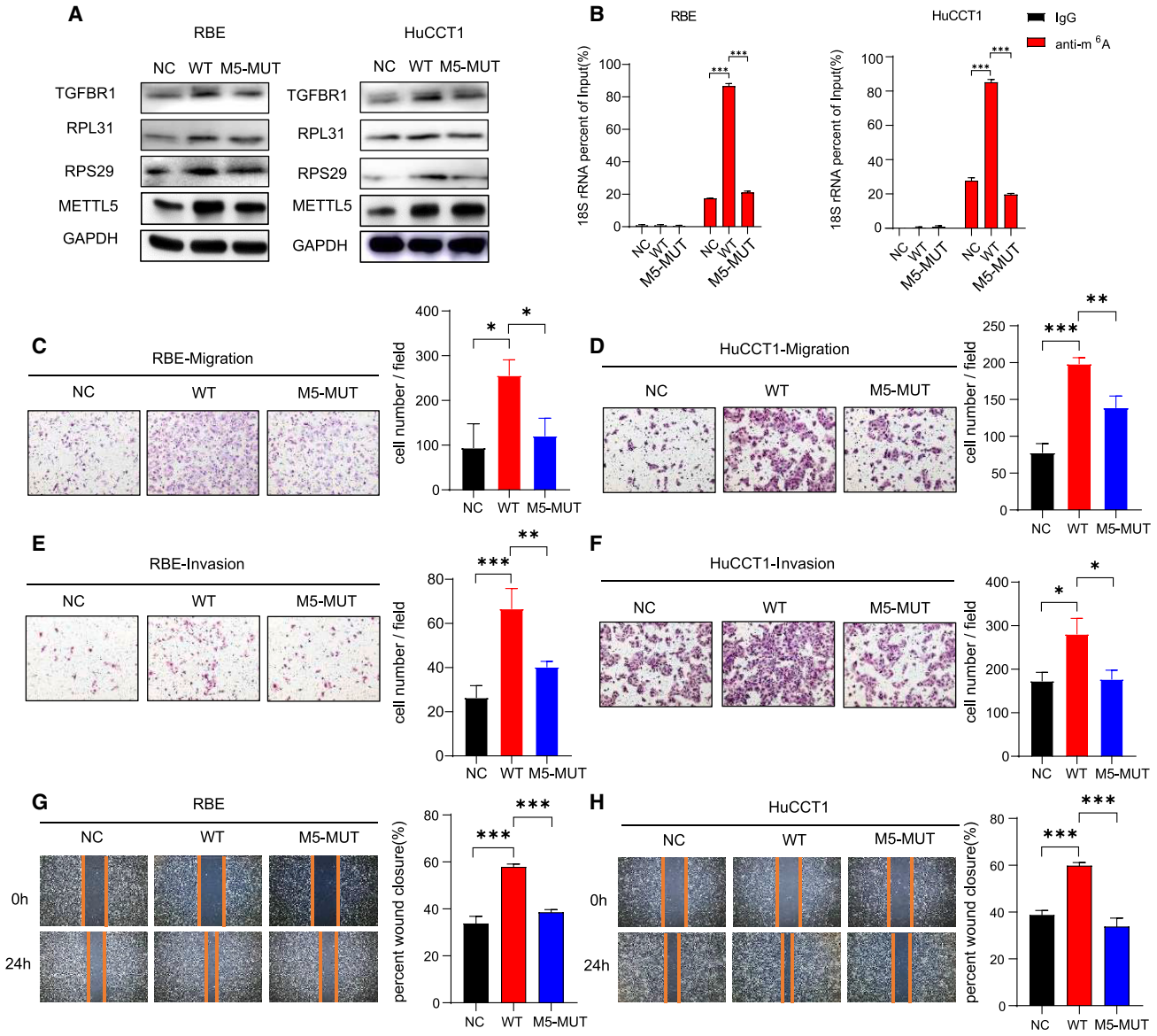

Figure 6. The 18S rRNA m6A modification methyltransferase activity is required for METTL5-mediated ICC progression

(A) Western blot assays examining WT and methyltransferase-inactive METTL5 overexpression as well as TGFBR1 and ribosome proteins expression in RBE (left) and HuCCT1 (right) cells. (B) Effects of forced expression of WT and methyltransferase-inactive METTL5 on 18S rRNA m^6A fraction levels in RBE (left) and HuCCT1 (right) cells determined by the m^6A-IP-qPCR method. (C and D) Cell migration analysis of RBE (C) and HuCCT1 (D) cells with forced expression of WT or methyltransferase-inactive METTL5. Left: representative images. Right: quantitative data. (E and F) Cell invasion analysis of RBE (E) and HuCCT1 (F) cells with forced expression of WT or methyltransferase-inactive METTL5. Left: representative images. Right: quantitative data. (G and H) Wound-healing assays of RBE (G) and HuCCT1 (H) cells with forced expression of WT or methyltransferase-inactive METTL5. Left: representative images. Right: quantitative data. Data presented as mean ± SD. *$p < 0.05$, **$p < 0.01$, ***$p < 0.001$ (one-way ANOVA). NC, empty vector; WT, overexpression of WT METTL5; M5-Mut, overexpression of methyltransferase-inactive mutant METTL5. Scale bar, 200 μm. All the *in vitro* assays were biologically repeated three times.

lines were cultured in 5% CO_2 incubators (Thermo Scientific, USA) at 37°C.

Animals

Six-week-old male NCG mice were purchased from GemPharmatech (Jiangsu, China). Male *Alb-Cre* transgenic mice (8 weeks old) were obtained from Shanghai Model Organisms Center. Female *Mettl5* $^{fl/wt}$ mice (8 weeks old) were purchased from Biocytogen (Beijing, China). All animal research was approved by the Institutional Ethics Committee for Clinical Research and Animal Trials of the First Affiliated Hospital of Sun Yat-Sen University and were in compliance with the Reporting of In Vivo Experiments (ARRIVE) guidelines.

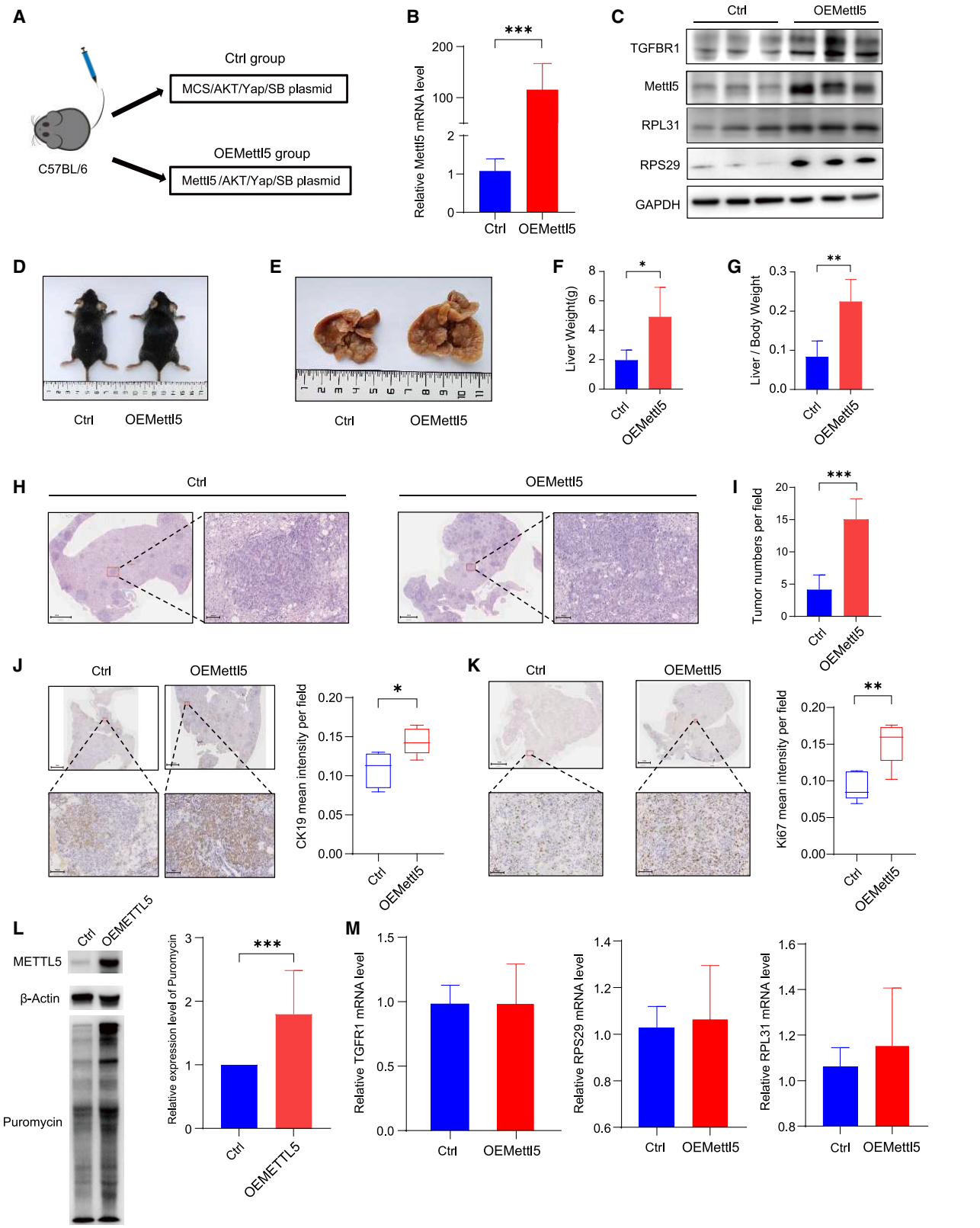

(legend on next page)

Plasmid construction, lentiviral transduction, and small interfering RNA knockdown

For overexpressing WT METTL5 and TGFBR1, full-length open reading frame (ORF) of human METTL5 gene (NM_001293186.2) and TGFBR1 (NM_001130916.3) were separately cloned into the pCDH vector. Methyltransferase inactive METTL5 plasmid was constructed by N126A and F129A mutation.[55] Lentiviral vectors expressing lentiCRISPR-NC and lentiCRISPR-METTL5 and lentiviral pLKO.1 METTL5 shRNAs were obtained from Horizon Discovery, China. To produce lentivirus, packaging vector pCMVDR8.9 and enveloped vector pCMV-VSVG were co-transfected with lentiviral vectors into HEK293T cells by Lipofectamine 3000 reagent (Invitrogen, USA). HuCCT1 and RBE cells were transfected with the lentivirus with 8 mg/mL Polybrene (Solarbio, China). The stable infected cells were selected with puromycin (2.5 mg/mL) (Solarbio, China). Finally, western blot assays were employed to examine the protein expression levels of METTL5 and TGFBR1. Small interfering RNAs (siRNAs) were purchased from Ribobio, China, and Lipofectamine 2000 was used to perform the siRNA transfection according to the manufacturer's protocol.

H&E and IHC staining

The H&E and IHC protocols were performed as previously described.[8,56] Briefly, ICC tissues were fixed for 24 h with 10% neutral buffered formalin and embed in paraffin. The paraffin-embedded tissues were then sliced into 4-mm-thick sections, were dewaxed in xylene, and then were rehydrated in a decreasing concentration gradient of ethanol. For H&E staining, the sections were subsequently stained with H&E. For IHC staining, the slides were heated for antigen retrieval for 2.5 min and were then blocked in 20% goat serum for 30 min, followed by incubation with primary antibodies targeting METTL5, CK19, and Ki67 overnight at 4°C. Real Envision Detection System (DAKO) was used to enlarge and visualize the protein signals according to the manufacturer's protocol. After hematoxylin staining, sections were separately dehydrated in increasing concentrations of ethanol and xylene. All slides were scanned by a ZEISS Axio Scan.Z1 Slide Scanner (AxioScan.Z1, ZEISS, German).

IHC data analysis

Integrated optical density (IOD), the cumulative value of the optical density (OD) and the area of the target region, was adopted to calculate the mean intensity per field (IOD/area) to reflect the target protein expression level. The exact IOD and area value were obtained using the Omage-Pro Plus 6.0 software (Media Cybernetics, https://www.mediacy.com/imageproplus). Briefly, the selected IHC image was loaded in the software and the background calibration was performed. Then the positive staining regions were labeled using the embedded color segmentation module based on the fixed threshold value of hue, saturation, and intensity (HSI). After the parameters were input, IOD and area values were outputted by the Measure module. The average value of intensity per field derived from five randomly selected regions of interest that were finally used as the index of target protein level. For the histological analysis, the normal bile ducts, blood vessels, and lymphatic vessels were recognized depending on morphological features. Histologically, the bile ducts are mainly located in the portal regions with small lumen-like structures and complete basilar membranes. Moreover, the inner walls of the bile ducts are lined with single cubic epithelial cells. For the small blood vessels, the inner walls are lined with single flat endothelial cells, in addition, erythrocytes can be observed in some blood vessels. The lymphatic vessels are also covered by the single flat endothelial cells in inner walls with incomplete basilar membranes. However, the lumen of lymphatic vessel is often irregular, showing a fissure-like, thin-walled structure. These vessel structures were differentiated according to the abovementioned key histological features.

RNA isolation, reverse transcription, and qRT-PCR

Total RNAs were extracted by TRIzol reagent (Invitrogen, USA). PrimeScript RT Reagent Kit (Takara, Japan) was used for reverse transcription. The cDNA samples were diluted and utilized for qRT-PCR using TB Green Premix Ex Taq II Kit (Takara, Japan) in the LightCycler 480 real-time PCR system (Roche, USA) according to the manufacturer's instructions. The housekeeping gene β-actin was used as an internal control to calculate relative mRNA expression levels. Each sample was repeated three times.

Anti-m^{6}A immunoprecipitation qPCR

The m^{6}A immunoprecipitation (IP)-qPCR assay was performed as previously described.[24] Briefly, total RNA was extracted from ICC tissues or cell lines using TRIzol. Total RNA of 2 μg was incubated with 5 μL of RNasin (40 U/μL), 100 μL of 5× IP buffer, and 2 μL of m6A-specific antibody or immunoglobulin (Ig) G in a final volume of 500 μL with DEPC H_2O at 4°C overnight. Protein A/G magnetic beads were washed twice with 1× IP buffer, blocked with BSA (0.5 mg/mL) for 2 h, and were then washed twice with 1× IP buffer. Subsequently, the beads were spun down and the supernatant was

Figure 7. Liver-specific overexpression of Mettl5 promotes ICC progression

(A) Diagram of experiment design. (B) mRNA level validation of Mettl5 overexpression (OEMettl5) in mouse livers using qRT-PCR assays. (C) Protein level examination of Mettl5 overexpression and TGFBR1 as well as ribosome protein expression in mouse livers using western blot assays. (D) Comparison of tumor burden in control and OEMettl5 mice at 4 weeks after plasmids transfection. (E) Representative gross images of control and OEMettl5 mouse livers. (F and G) Comparison of tumor burden indicated by the liver weight (F) and the ratio of liver weight to body weight (G) between control and OEMettl5 mice. (H and I) Representative images of H&E staining of control and OEMettl5 mouse livers (H). The numbers of tumor lesions in control and OEMettl5 mouse livers were evaluated and compared (I). Scale bar, 2 mm (H, left). Scale bar, 100 μm (H, right). (J and K) IHC staining of CK19 (J) and Ki67 (K) in control and OEMettl5 mouse livers (left). The corresponding statistical data are shown (right). Scale bar, 1 mm (J and K, top). Scale bar, 100 μm (J and K, bottom). (L) Puromycin intake assay of global translation level in livers of control and OEMettl5 mice (left). The quantitative data are shown on the right. (M) qRT-PCR analysis mRNA levels of TGFBR1 and ribosome proteins in livers of control and OEMettl5 mice. Data presented as mean ± SD. $^{**}p < 0.01$, $^{***}p < 0.001$ (log-rank test; Student's t test). oe, overexpression; Mut, catalytic inactive mutant; A/Y+C, AKT/YapS127A + control plasmid; A/Y+M5, AKT/YapS127A + Mettl5 overexpression plasmid. Scale bar, 50 μm. All the *in vitro* assays were biologically repeated three times.

discarded. The above reactions were transferred to washed beads and were incubated with the beads at 4°C for 2 h. Thereafter, the beads were spun down followed by removing the supernatant. The beads were subjected to TRIzol for further RNA extraction and qRT-PCR assays using 18S rRNA primers.

SELECT method

SELECT was performed according to Epi-SELECT m^6A site identification kit (EP-biotek, China). Briefly, the designed up and down probes flanking the m^6A modification site at position 1,832 were annealed, followed by extension of a single base using SELECT DNA polymerase and nicking of the junction using SELECT Ligase. qPCR assays were then performed to measure the m^6A level at the targeted site. The probes and primers used for SELECT in the study are provided below: up probe, tagccagtaccgtagtgcgtgCACCTACGGAAACCTTG; down probe, TACGACTTTTACTTCCTCTAcagaggctgagtcgctgcat; qRT-PCR forward primer, 5′-ATGCAGCGACTCAGCCTCTG-3′; qRT-PCR reverse primer, 5′-TAGCCAGTACCGTAGTGCGTG-3′.

Liquid chromatograph-mass spectrometry

Total cell RNA samples of 2 μg were electrophoresed at 100 V for 20 min in Tris-borate-EDTA (TBE) solution using 1.5% agarose gel. Under ultraviolet light, 28S and 18S rRNA were separated by gel cutting and were extracted from the gel using a ZR small-RNA PAGE Recovery kit (Zymo Research, R1070). Total mRNA was extracted using a commercial mRNA isolation kit based on oligo-dT cellulose method. After RNA isolation, 50 ng of recovered small RNAs were diluted and added to 20 mM NH4OAc and 1 U of nuclease P1 (sigma, N8630-1VL). The mixtures were then incubated at 42°C for 2 h, followed by adding 1 μL of FastAP Thermo-sensitive alkaline phosphatase (Thermo, EF0651) and 2.3 μL of 10× FastAP buffer and incubation at 37°C for 2 h. Finally, the digested RNA was diluted twice with enzyme-free water and filtered through a 0.22-μm filter (Millipore, SLGVR04NL). The 5-μL sample was injected and metabolite separation was performed on Agilent InfinityLab Poroshell 120 SB-C18 column (100 × 2.1 mm, 2.7-mm particle size). Liquid chromatograph (LC) gradient was generated using LC solvents A (water containing 0.1% formic acid) and B (methanol). Autosampler temperature was set at 10°C and the column temperature was set at 35°C. Mass spectrometry analysis was performed with a Product mode for measurement of samples (m/z 268.1040 → 136.0618 for adenosine and 282.1197 → 150.0775 for m6A, positive electrospray ionization mode).

Western blot

Total proteins were extracted by cell lysis buffer (CST) in the presence of phosphatase inhibitor (Sigma, Germany) and protease inhibitor (Sigma, Germany). The protein concentration was measured by the BCA Protein Assay Kit (Epizyme, China). Protein samples were then separated on a PAGE gel by electrophoresis and then blotted onto polyvinylidene fluoride (PVDF) membranes (GE Healthcare). Blots were incubated with the primary antibodies overnight at 4°C, followed by the secondary antibody for 1 h at room temperature. Omni-ECL Femto Light Chemiluminescence Kit (Epizyme, China) were used to visualize the protein bands.

Cell migration and invasion assays

Cell migration and invasion assays were performed using 24-well plates containing 8-mm pore size chamber inserts (Corning, USA). For migration assay, 5×10^4 cells in 500 μL of serum-free medium were added into the upper chamber. For invasion assay, the membranes were pre-coated with 100 μL of 10% Matrigel (Corning, USA), followed by the adding of 5×10^4 cells into the upper chamber. A total of 750 μL of cell culture medium supplemented with 10% fetal bovine serum was then added in the lower chambers. After cell culture for 24 h, the upper chambers were collected and stained with 0.5% crystal violet. Each assay was repeated three times and the migrated cells were counted in five random fields of each chamber under the bright field of a microscope (Olympus, Japan).

Wound-healing assay

In brief, a total of 1×10^6 cells were seeded into a six-well plate. When the cell number approximately covered 80% of the plate surface, a straining line was painted on each well. The wound width was measured every 12 h over a period of 24 h under the bright field of a microscope (Olympus, Japan). Values were expressed as the percentage of wound closure, which was calculated as follows: percentage of wound closure = $1 - (\text{width}_t/\text{width}_0) \times 100\%$

Cell viability assay

The cell viability assay was performed by MTX (Promega, Madison, WI) according to the manufacturer's instructions. Briefly, 1.5×10^3 cells per well were seeded into a 96-well plate. Then 100 μL of culture medium and 20 μL of MTX were mixed and were then added into the cells at indicated time points. The mixture was incubated at 37°C for 2 h, and the OD was measured at 450-nm wavelength.

In vitro and *in vivo* puromycin intake assay

Puromycin intake assay was performed as previously described.[57] For the *in vitro* assays, the ICC cells were incubated with puromycin (1 μM final concentration) for 30 min, followed by protein extraction and western blot examination using anti-puromycin antibody (MABE343, Millipore). For the *in vivo* assays, mice were injected with 40 nmol puromycin/g body weight intravenously. The tumor tissues were harvested at 10 min after puromycin injection and were examined by western blot assays. The expression of housekeeping gene was used as control.

Ribosome nascent-chain RNC-seq

RNC-seq was performed as previously described.[58] In brief, 5×10^6 cells were treated with 100 mg/mL cycloheximide in 37°C for 15 min and were then lysed by 1 mL of cell lysis buffer on ice for 30 min. Supernatant of cell lysates was collected after centrifuging at 16,200 × *g* for 10 min at 4°C. Then 10% of the extraction was used as input control. The remaining extraction was layered onto 10 mL of sucrose buffer and was then ultra-centrifuged at 174,900 × *g* for 5 h at 4°C in an SW32 rotor (Beckman Coulter,

USA). RNC pellets that contained the polysome fractions were on the bottom of the centrifuge tube after ultracentrifugation. RNAs of RNC and the input samples were extracted by TRIzol reagent for RNA-seq and qRT-PCR assays to examine the gene expression.[59] Buffer ingredients were prepared as follows: ribosome buffer (RB buffer), 20 mM HEPES-KOH (pH 7.4), 15 mM $MgCl_2$, 200 mM KCl, 100 mg/mL cycloheximide, and 2mM dithiothreitol; cell lysis buffer, 1% Triton X-100 in RB buffer; sucrose buffer, 30% sucrose in RB buffer.

RNC-seq data analysis

The cDNA library construction and sequencing were performed by the Beijing Genomics Institute using BGISEQ-500 platform (BGI Shenzhen, China) as previously described.[60] High-quality reads were mapped to University of California, Santa Cruz (UCSC) human reference genome (GRCh37/hg19) using the alignment tool Hisat2. The gene expression level was normalized by using the transcripts per kilobase of exon model per million mapped reads (TPM) method. Genes with TPM > 0.1 were selected for further analysis. TRs were calculated using the following formula: TR = (TPM in RNC-seq)/(TPM in input RNA-seq). The genes with abs (log2-fold change) >1 in translation efficiency were considered as the differentially translating genes. Pathway analysis was conducted using the enrichWP function of the clusterProfiler package. The list of G4-containing mRNAs was obtained from Yang et al.[31] Pathway analysis was conducted using the Wikipathway of the WEB-based Gene Set Analysis Toolkit (WebGestalt) (http://www.webgestalt.org/).

Caudal vein injection mouse metastasis model

A total of 1×10^6 HuCCT1-sgNC and HuCCT1-sgMETTL5 cells in 0.2 mL of PBS were separately injected into 6-week-old male NCG mice (N = 7 per group) via caudal vein. Mice were sacrificed at 4 weeks after injection, and the lung tissues were processed into 4-mm-thick paraffin-embedded sections. H&E staining was subsequently performed to determine the pulmonary metastasis.

Generation of liver-specific conditional Mettl5-knockout mice

Alb-Cre Mettl5$^{fl/fl}$ mice were obtained by crossing 8-week-old male *Alb-Cre* mice with 8-week-old female *Mettl5*$^{fl/wt}$ mice (homozygous liver-specific conditional Mettl5-knockout mice); DNA extracted from mouse tail (Mouse Tail Direct PCR Kit, FOREGENE) was used for genotype identification and, after amplification of target DNA, the result was visualized by agarose gel electrophoresis. Primers for floxed Mettl5-knockout allele genotyping were 5′-loxP forward (5′-ATACA CACTCCTGGCCACT-CCTTGT-3′), 5′-loxP reverse (5′-CCCTGGC TTCTAGGGTGTGAATCAG-3′), 3′-loxP forward (5′-TGGAGAGCC TCCACCTTCCTTCTAC-3′), and 3′-loxP reverse (5′-AGACCATGA GAGGGTGGAGCAGAAT-3′). Primers for *Alb-Cre* transgenic genotyping were forward (5′-TGCTTCTGTCCGTTTGCCGGT-3′) and reverse (5′- CTAAGTGCCTTCTCTACACCT-3′).

AKT/YapS127A-induced mouse ICC model using hydrodynamic transfection

An AKT/YapS127A-induced mouse ICC model used to investigate the effect of interested genes on tumor biology has been reported.[8] To establish the ICC mouse model in wide-type or Mettl5-knockout mice, 20 mg of pT3-myr-AKT-HA (Addgene #31789), 30 mg of pT3-EF1aH Yap S127A (Addgene #86497) and SB transposase plasmid (1/10–25 of the total oncogene plasmids) (Addgene) were mixed and diluted in 2 mL of saline and were then injected into the tail vein of 6-week-old mice within 7 s. For overexpression of Mettl5, 20 mg of pT3-EF1a-HA-Mettl5 plasmid was additionally added into the abovementioned plasmid mixtures and was then injected into the tail vein of 6-week-old male C57BL/6J WT mice. Mice were sacrificed at 4 or 6 weeks later; the liver was dissected and processed into paraffin-embedded sections for the analysis of ICC tumorigenesis and progression.

Statistical analysis

All statistical tests and sample sizes are included in the figure legends or methods. All data are shown as mean ± SD. In all cases, the p values are represented as follows: ***$p < 0.001$, **$p < 0.01$, *$p < 0.05$, and not statistically significant when $p > 0.05$. Unless otherwise stated, statistical significance was calculated as appropriate using unpaired, two-tailed Student's t test or one-way ANOVA. Statistical analyses were performed using GraphPad Prism 7.

DATA AND CODE AVAILABILITY

Data are available on reasonable request.

SUPPLEMENTAL INFORMATION

Supplemental information can be found online at https://doi.org/10.1016/j.ymthe.2023.09.014.

ACKNOWLEDGMENTS

This work was supported by National Key Research and Development Program of China (2022YFE0138700 to S.B.L.), National Natural Science Foundation of China (82130083 and 81825013 to M.K., 82325036 and81974435 to S.B.L., 82103600 to Z.H.D., 82202949 to J.B.L), and Fundamental Research Funds for the Central Universities, Sun Yat-sen University (23ykzy004 to S.B.L). We would like to thank all patients who generously donated the tissues. We sincerely thank Dr. Jialin Wu for the painting guidance of graphic abstract production, Dr. Huanjing Hu for the suggestion on RNC-seq data analysis, and Dr. Lili Chen for the suggestion on histological analysis of IHC assays.

AUTHOR CONTRIBUTIONS

Z.H.D., W.J.Z., Y.D.H., and X.Y.Z. performed the *in vitro* assays. Z.H.D., Y.D.H., and W.J.Z. contributed to the *in vivo* animal experiments. X.Y.Z., J.B.L., and S.B.L. performed RNC-seq and data analysis. Y.F.Z., K.L., Z.H.C., H.N.L., and S.P. developed protocols and coordinated tissue collection. M.K. supervised the study and, together with S.B.L. and S.Q.L., coordinated the project, designed experiments, analyzed and interpreted data. Z.H.D. and W.J.Z. wrote the draft, and all of the authors revised and modified the final manuscript.

DECLARATION OF INTERESTS

The authors declare no competing interests.

REFERENCES

1. Valle, J.W., Kelley, R.K., Nervi, B., Oh, D.-Y., and Zhu, A.X. (2021). Biliary tract cancer. Lancet Lond. Engl. *397*, 428–444. https://doi.org/10.1016/S0140-6736(21)00153-7.
2. Banales, J.M., Marin, J.J.G., Lamarca, A., Rodrigues, P.M., Khan, S.A., Roberts, L.R., Cardinale, V., Carpino, G., Andersen, J.B., Braconi, C., et al. (2020). Cholangiocarcinoma 2020: the next horizon in mechanisms and management. Nat. Rev. Gastroenterol. Hepatol. *17*, 557–588. https://doi.org/10.1038/s41575-020-0310-z.
3. Abou-Alfa, G.K., Sahai, V., Hollebecque, A., Vaccaro, G., Melisi, D., Al-Rajabi, R., Paulson, A.S., Borad, M.J., Gallinson, D., Murphy, A.G., et al. (2020). Pemigatinib for previously treated, locally advanced or metastatic cholangiocarcinoma: a multicentre, open-label, phase 2 study. Lancet Oncol. *21*, 671–684. https://doi.org/10.1016/S1470-2045(20)30109-1.
4. Barbieri, I., and Kouzarides, T. (2020). Role of RNA modifications in cancer. Nat. Rev. Cancer *20*, 303–322. https://doi.org/10.1038/s41568-020-0253-2.
5. Zhao, B.S., Roundtree, I.A., and He, C. (2017). Post-transcriptional gene regulation by mRNA modifications. Nat. Rev. Mol. Cell Biol. *18*, 31–42. https://doi.org/10.1038/nrm.2016.132.
6. Su, R., Dong, L., Li, C., Nachtergaele, S., Wunderlich, M., Qing, Y., Deng, X., Wang, Y., Weng, X., Hu, C., et al. (2018). R-2HG Exhibits Anti-tumor Activity by Targeting FTO/m6A/MYC/CEBPA Signaling. Cell *172*, 90–105.e23. https://doi.org/10.1016/j.cell.2017.11.031.
7. Su, T., Huang, M., Liao, J., Lin, S., Yu, P., Yang, J., Cai, Y., Zhu, S., Xu, L., Peng, Z., et al. (2021). Insufficient Radiofrequency Ablation Promotes Hepatocellular Carcinoma Metastasis Through N6-Methyladenosine mRNA Methylation-Dependent Mechanism. Hepatol. Baltim. Md. *74*, 1339–1356. https://doi.org/10.1002/hep.31766.
8. Dai, Z., Liu, H., Liao, J., Huang, C., Ren, X., Zhu, W., Zhu, S., Peng, B., Li, S., Lai, J., et al. (2021). N7-Methylguanosine tRNA modification enhances oncogenic mRNA translation and promotes intrahepatic cholangiocarcinoma progression. Mol. Cell *81*, 3339–3355.e8. https://doi.org/10.1016/j.molcel.2021.07.003.
9. Orellana, E.A., Liu, Q., Yankova, E., Pirouz, M., De Braekeleer, E., Zhang, W., Lim, J., Aspris, D., Sendinc, E., Garyfallos, D.A., et al. (2021). METTL1-mediated m7G modification of Arg-TCT tRNA drives oncogenic transformation. Mol. Cell *81*, 3323–3338.e14. https://doi.org/10.1016/j.molcel.2021.06.031.
10. Cui, Q., Yin, K., Zhang, X., Ye, P., Chen, X., Chao, J., Meng, H., Wei, J., Roeth, D., Li, L., et al. (2021). Targeting PUS7 suppresses tRNA pseudouridylation and glioblastoma tumorigenesis. Nat. Cancer *2*, 932–949. https://doi.org/10.1038/s43018-021-00238-0.
11. Piekna-Przybylska, D., Decatur, W.A., and Fournier, M.J. (2008). The 3D rRNA modification maps database: with interactive tools for ribosome analysis. Nucleic Acids Res. *36*, D178–D183. https://doi.org/10.1093/nar/gkm855.
12. Sloan, K.E., Warda, A.S., Sharma, S., Entian, K.-D., Lafontaine, D.L.J., and Bohnsack, M.T. (2017). Tuning the ribosome: The influence of rRNA modification on eukaryotic ribosome biogenesis and function. RNA Biol. *14*, 1138–1152. https://doi.org/10.1080/15476286.2016.1259781.
13. Kan, G., Wang, Z., Sheng, C., Chen, G., Yao, C., Mao, Y., and Chen, S. (2021). Dual Inhibition of DKC1 and MEK1/2 Synergistically Restrains the Growth of Colorectal Cancer Cells. Adv. Sci. *8*, 2004344. https://doi.org/10.1002/advs.202004344.
14. Balogh, E., Chandler, J.C., Varga, M., Tahoun, M., Menyhárd, D.K., Schay, G., Goncalves, T., Hamar, R., Légrádi, R., Szekeres, Á., et al. (2020). Pseudouridylation defect due to DKC1 and NOP10 mutations causes nephrotic syndrome with cataracts, hearing impairment, and enterocolitis. Proc. Natl. Acad. Sci. USA *117*, 15137–15147. https://doi.org/10.1073/pnas.2002328117.
15. Shinde, H., Dudhate, A., Kadam, U.S., and Hong, J.C. (2023). RNA methylation in plants: An overview. Front. Plant Sci. *14*, 1132959. https://doi.org/10.3389/fpls.2023.1132959.
16. Manduzio, S., and Kang, H. (2021). RNA methylation in chloroplasts or mitochondria in plants. RNA Biol. *18*, 2127–2135. https://doi.org/10.1080/15476286.2021.1909321.
17. Sharma, B., Prall, W., Bhatia, G., and Gregory, B.D. (2023). The Diversity and Functions of Plant RNA Modifications: What We Know and Where We Go from Here. Annu. Rev. Plant Biol. *74*, 53–85. https://doi.org/10.1146/annurev-arplant-071122-085813.
18. Liberman, N., O'Brown, Z.K., Earl, A.S., Boulias, K., Gerashchenko, M.V., Wang, S.Y., Fritsche, C., Fady, P.-E., Dong, A., Gladyshev, V.N., and Greer, E.L. (2020). N6-adenosine methylation of ribosomal RNA affects lipid oxidation and stress resistance. Sci. Adv. *6*, eaaz4370. https://doi.org/10.1126/sciadv.aaz4370.
19. Ma, H., Wang, X., Cai, J., Dai, Q., Natchiar, S.K., Lv, R., Chen, K., Lu, Z., Chen, H., Shi, Y.G., et al. (2019). N6-Methyladenosine methyltransferase ZCCHC4 mediates ribosomal RNA methylation. Nat. Chem. Biol. *15*, 88–94. https://doi.org/10.1038/s41589-018-0184-3.
20. Sergiev, P.V., Aleksashin, N.A., Chugunova, A.A., Polikanov, Y.S., and Dontsova, O.A. (2018). Structural and evolutionary insights into ribosomal RNA methylation. Nat. Chem. Biol. *14*, 226–235. https://doi.org/10.1038/nchembio.2569.
21. Liu, N., Parisien, M., Dai, Q., Zheng, G., He, C., and Pan, T. (2013). Probing N6-methyladenosine RNA modification status at single nucleotide resolution in mRNA and long noncoding RNA. RNA N. Y. N. *19*, 1848–1856. https://doi.org/10.1261/rna.041178.113.
22. Xing, M., Liu, Q., Mao, C., Zeng, H., Zhang, X., Zhao, S., Chen, L., Liu, M., Shen, B., Guo, X., et al. (2020). The 18S rRNA m6 A methyltransferase METTL5 promotes mouse embryonic stem cell differentiation. EMBO Rep. *21*, e49863. https://doi.org/10.15252/embr.201949863.
23. Ignatova, V.V., Stolz, P., Kaiser, S., Gustafsson, T.H., Lastres, P.R., Sanz-Moreno, A., Cho, Y.-L., Amarie, O.V., Aguilar-Pimentel, A., Klein-Rodewald, T., et al. (2020). The rRNA m6A methyltransferase METTL5 is involved in pluripotency and developmental programs. Genes Dev. *34*, 715–729. https://doi.org/10.1101/gad.333369.119.
24. Peng, H., Chen, B., Wei, W., Guo, S., Han, H., Yang, C., Ma, J., Wang, L., Peng, S., Kuang, M., and Lin, S. (2022). N6-methyladenosine (m6A) in 18S rRNA promotes fatty acid metabolism and oncogenic transformation. Nat. Metab. *4*, 1041–1054. https://doi.org/10.1038/s42255-022-00622-9.
25. Rong, B., Zhang, Q., Wan, J., Xing, S., Dai, R., Li, Y., Cai, J., Xie, J., Song, Y., Chen, J., et al. (2020). Ribosome 18S m6A Methyltransferase METTL5 Promotes Translation Initiation and Breast Cancer Cell Growth. Cell Rep. *33*, 108544. https://doi.org/10.1016/j.celrep.2020.108544.
26. Rong, Z.-X., Li, Z., He, J.-J., Liu, L.-Y., Ren, X.-X., Gao, J., Mu, Y., Guan, Y.-D., Duan, Y.-M., Zhang, X.-P., et al. (2019). Downregulation of Fat Mass and Obesity Associated (FTO) Promotes the Progression of Intrahepatic Cholangiocarcinoma. Front. Oncol. *9*, 369. https://doi.org/10.3389/fonc.2019.00369.
27. Huang, X., Zhu, L., Wang, L., Huang, W., Tan, L., Liu, H., Huo, J., Su, T., Zhang, M., Kuang, M., et al. (2022). YTHDF1 promotes intrahepatic cholangiocarcinoma progression via regulating EGFR mRNA translation. J. Gastroenterol. Hepatol. *37*, 1156–1168. https://doi.org/10.1111/jgh.15816.
28. Jansson, M.D., Häfner, S.J., Altinel, K., Tehler, D., Krogh, N., Jakobsen, E., Andersen, J.V., Andersen, K.L., Schoof, E.M., Ménard, P., et al. (2021). Regulation of translation by site-specific ribosomal RNA methylation. Nat. Struct. Mol. Biol. *28*, 889–899. https://doi.org/10.1038/s41594-021-00669-4.
29. Varshney, D., Spiegel, J., Zyner, K., Tannahill, D., and Balasubramanian, S. (2020). The regulation and functions of DNA and RNA G-quadruplexes. Nat. Rev. Mol. Cell Biol. *21*, 459–474. https://doi.org/10.1038/s41580-020-0236-x.
30. Feng, Y., Zhang, F., Lokey, L.K., Chastain, J.L., Lakkis, L., Eberhart, D., and Warren, S.T. (1995). Translational suppression by trinucleotide repeat expansion at FMR1. Science *268*, 731–734. https://doi.org/10.1126/science.7732383.
31. Yang, S.Y., Lejault, P., Chevrier, S., Boidot, R., Robertson, A.G., Wong, J.M.Y., and Monchaud, D. (2018). Transcriptome-wide identification of transient RNA G-quadruplexes in human cells. Nat. Commun. *9*, 4730. https://doi.org/10.1038/s41467-018-07224-8.
32. Gao, L., Hu, Y., Tian, Y., Fan, Z., Wang, K., Li, H., Zhou, Q., Zeng, G., Hu, X., Yu, L., et al. (2019). Lung cancer deficient in the tumor suppressor GATA4 is sensitive to TGFBR1 inhibition. Nat. Commun. *10*, 1665. https://doi.org/10.1038/s41467-019-09295-7.
33. Guda, K., Natale, L., Lutterbaugh, J., Wiesner, G.L., Lewis, S., Tanner, S.M., Tomsic, J., Valle, L., de la Chapelle, A., Elston, R.C., et al. (2009). Infrequent detection of germline allele-specific expression of TGFBR1 in lymphoblasts and tissues of colon cancer

patients. Cancer Res. *69*, 4959–4961. https://doi.org/10.1158/0008-5472.CAN-09-0225.

34. Song, X., Liu, X., Wang, H., Wang, J., Qiao, Y., Cigliano, A., Utpatel, K., Ribback, S., Pilo, M.G., Serra, M., et al. (2019). Combined CDK4/6 and Pan-mTOR Inhibition Is Synergistic Against Intrahepatic Cholangiocarcinoma. Clin. Cancer Res. *25*, 403–413. https://doi.org/10.1158/1078-0432.CCR-18-0284.

35. Zhang, S., Song, X., Cao, D., Xu, Z., Fan, B., Che, L., Hu, J., Chen, B., Dong, M., Pilo, M.G., et al. (2017). Pan-mTOR inhibitor MLN0128 is effective against intrahepatic cholangiocarcinoma in mice. J. Hepatol. *67*, 1194–1203. https://doi.org/10.1016/j.jhep.2017.07.006.

36. Schosserer, M., Minois, N., Angerer, T.B., Amring, M., Dellago, H., Harreither, E., Calle-Perez, A., Pircher, A., Gerstl, M.P., Pfeifenberger, S., et al. (2015). Methylation of ribosomal RNA by NSUN5 is a conserved mechanism modulating organismal lifespan. Nat. Commun. *6*, 6158. https://doi.org/10.1038/ncomms7158.

37. van Tran, N., Ernst, F.G.M., Hawley, B.R., Zorbas, C., Ulryck, N., Hackert, P., Bohnsack, K.E., Bohnsack, M.T., Jaffrey, S.R., Graille, M., and Lafontaine, D.L.J. (2019). The human 18S rRNA m6A methyltransferase METTL5 is stabilized by TRMT112. Nucleic Acids Res. *47*, 7719–7733. https://doi.org/10.1093/nar/gkz619.

38. Richard, E.M., Polla, D.L., Assir, M.Z., Contreras, M., Shahzad, M., Khan, A.A., Razzaq, A., Akram, J., Tarar, M.N., Blanpied, T.A., et al. (2019). Bi-allelic Variants in METTL5 Cause Autosomal-Recessive Intellectual Disability and Microcephaly. Am. J. Hum. Genet. *105*, 869–878. https://doi.org/10.1016/j.ajhg.2019.09.007.

39. Leismann, J., Spagnuolo, M., Pradhan, M., Wacheul, L., Vu, M.A., Musheev, M., Mier, P., Andrade-Navarro, M.A., Graille, M., Niehrs, C., et al. (2020). The 18S ribosomal RNA m6 A methyltransferase Mettl5 is required for normal walking behavior in Drosophila. EMBO Rep. *21*, e49443. https://doi.org/10.15252/embr.201949443.

40. Wang, L., Liang, Y., Lin, R., Xiong, Q., Yu, P., Ma, J., Cheng, M., Han, H., Wang, X., Wang, G., et al. (2022). Mettl5 mediated 18S rRNA N6-methyladenosine (m6A) modification controls stem cell fate determination and neural function. Genes Dis. *9*, 268–274. https://doi.org/10.1016/j.gendis.2020.07.004.

41. Liu, X., Ma, H., Ma, L., Li, K., and Kang, Y. (2022). The potential role of methyltransferase-like 5 in deficient mismatch repair of uterine corpus endometrial carcinoma. Bioengineered *13*, 5525–5536. https://doi.org/10.1080/21655979.2022.2036912.

42. Zhang, Z., Zhang, C., Luo, Y., Wu, P., Zhang, G., Zeng, Q., Wang, L., Yang, Z., Xue, L., Zheng, B., et al. (2021). m6A regulator expression profile predicts the prognosis, benefit of adjuvant chemotherapy, and response to anti-PD-1 immunotherapy in patients with small-cell lung cancer. BMC Med. *19*, 284. https://doi.org/10.1186/s12916-021-02148-5.

43. Zhang, Z., Zhang, C., Yang, Z., Zhang, G., Wu, P., Luo, Y., Zeng, Q., Wang, L., Xue, Q., Zhang, Y., et al. (2021). m6A regulators as predictive biomarkers for chemotherapy benefit and potential therapeutic targets for overcoming chemotherapy resistance in small-cell lung cancer. J. Hematol. Oncol. *14*, 190. https://doi.org/10.1186/s13045-021-01173-4.

44. Wang, Z., Liu, J., Yang, Y., Xing, C., Jing, J., and Yuan, Y. (2021). Expression and prognostic potential of ribosome 18S RNA m6A methyltransferase METTL5 in gastric cancer. Cancer Cell Int. *21*, 569. https://doi.org/10.1186/s12935-021-02274-3.

45. Huang, H., Li, H., Pan, R., Wang, S., Khan, A.A., Zhao, Y., Zhu, H., and Liu, X. (2022). Ribosome 18S m6A methyltransferase METTL5 promotes pancreatic cancer progression by modulating c-Myc translation. Int. J. Oncol. *60*, 9. https://doi.org/10.3892/ijo.2021.5299.

46. Polikanov, Y.S., Melnikov, S.V., Söll, D., and Steitz, T.A. (2015). Structural insights into the role of rRNA modifications in protein synthesis and ribosome assembly. Nat. Struct. Mol. Biol. *22*, 342–344. https://doi.org/10.1038/nsmb.2992.

47. Basu, A., Das, P., Chaudhuri, S., Bevilacqua, E., Andrews, J., Barik, S., Hatzoglou, M., Komar, A.A., and Mazumder, B. (2011). Requirement of rRNA methylation for 80S ribosome assembly on a cohort of cellular internal ribosome entry sites. Mol. Cell. Biol. *31*, 4482–4499. https://doi.org/10.1128/MCB.05804-11.

48. Baxter-Roshek, J.L., Petrov, A.N., and Dinman, J.D. (2007). Optimization of ribosome structure and function by rRNA base modification. PLoS One *2*, e174. https://doi.org/10.1371/journal.pone.0000174.

49. Demirci, H., Murphy, F., Belardinelli, R., Kelley, A.C., Ramakrishnan, V., Gregory, S.T., Dahlberg, A.E., and Jogl, G. (2010). Modification of 16S ribosomal RNA by the KsgA methyltransferase restructures the 30S subunit to optimize ribosome function. RNA N. Y. N. *16*, 2319–2324. https://doi.org/10.1261/rna.2357210.

50. Yoon, A., Peng, G., Brandenburger, Y., Zollo, O., Xu, W., Rego, E., and Ruggero, D. (2006). Impaired control of IRES-mediated translation in X-linked dyskeratosis congenita. Science *312*, 902–906. https://doi.org/10.1126/science.1123835.

51. Cammas, A., and Millevoi, S. (2017). RNA G-quadruplexes: emerging mechanisms in disease. Nucleic Acids Res. *45*, 1584–1595. https://doi.org/10.1093/nar/gkw1280.

52. Rizvi, S., Khan, S.A., Hallemeier, C.L., Kelley, R.K., and Gores, G.J. (2018). Cholangiocarcinoma - evolving concepts and therapeutic strategies. Nat. Rev. Clin. Oncol. *15*, 95–111. https://doi.org/10.1038/nrclinonc.2017.157.

53. Yang, H., Ye, D., Guan, K.-L., and Xiong, Y. (2012). IDH1 and IDH2 mutations in tumorigenesis: mechanistic insights and clinical perspectives. Clin. Cancer Res. *18*, 5562–5571. https://doi.org/10.1158/1078-0432.CCR-12-1773.

54. Abou-Alfa, G.K., Macarulla, T., Javle, M.M., Kelley, R.K., Lubner, S.J., Adeva, J., Cleary, J.M., Catenacci, D.V., Borad, M.J., Bridgewater, J., et al. (2020). Ivosidenib in IDH1-mutant, chemotherapy-refractory cholangiocarcinoma (ClarIDHy): a multicentre, randomised, double-blind, placebo-controlled, phase 3 study. Lancet Oncol. *21*, 796–807. https://doi.org/10.1016/S1470-2045(20)30157-1.

55. Bheemanaik, S., Reddy, Y.V.R., and Rao, D.N. (2006). Structure, function and mechanism of exocyclic DNA methyltransferases. Biochem. J. *399*, 177–190. https://doi.org/10.1042/BJ20060854.

56. Dai, Z., Wang, Z., Lei, K., Liao, J., Peng, Z., Lin, M., Liang, P., Yu, J., Peng, S., Chen, S., and Kuang, M. (2021). Irreversible electroporation induces CD8+ T cell immune response against post-ablation hepatocellular carcinoma growth. Cancer Lett. *503*, 1–10. https://doi.org/10.1016/j.canlet.2021.01.001.

57. Schmidt, E.K., Clavarino, G., Ceppi, M., and Pierre, P. (2009). SUnSET, a nonradioactive method to monitor protein synthesis. Nat. Methods *6*, 275–277. https://doi.org/10.1038/nmeth.1314.

58. Wang, T., Cui, Y., Jin, J., Guo, J., Wang, G., Yin, X., He, Q.-Y., and Zhang, G. (2013). Translating mRNAs strongly correlate to proteins in a multivariate manner and their translation ratios are phenotype specific. Nucleic Acids Res. *41*, 4743–4754. https://doi.org/10.1093/nar/gkt178.

59. Kadam, U.S., Lossie, A.C., Schulz, B., and Joseph, I. (2013). Gene Expression Analysis Using Conventional and Imaging Methods. In DNA and RNA Nanobiotechnologies in Medicine: Diagnosis and Treatment of Diseases. RNA Technologies (Springer).

60. Chen, K., Liu, J., Liu, S., Xia, M., Zhang, X., Han, D., Jiang, Y., Wang, C., and Cao, X. (2017). Methyltransferase SETD2-Mediated Methylation of STAT1 Is Critical for Interferon Antiviral Activity. Cell *170*, 492–506.e14. https://doi.org/10.1016/j.cell.2017.06.042.